RNA machinery –the ribosome

October 20, 2009

Professor Wilma K. Olson

Structural overview of the ribosome

The ribosome, the protein machinery responsible for protein synthesis, is made up of a small (30S) and a large (50S) subunit.

The small subunit controls information throughput during protein synthesis — finding the mRNA strand, combining with the large subunit, ensuring that each codon in the message pairs with tRNA anticodon.

1fka (Yonath)
1fkg (Ramakrishnan)
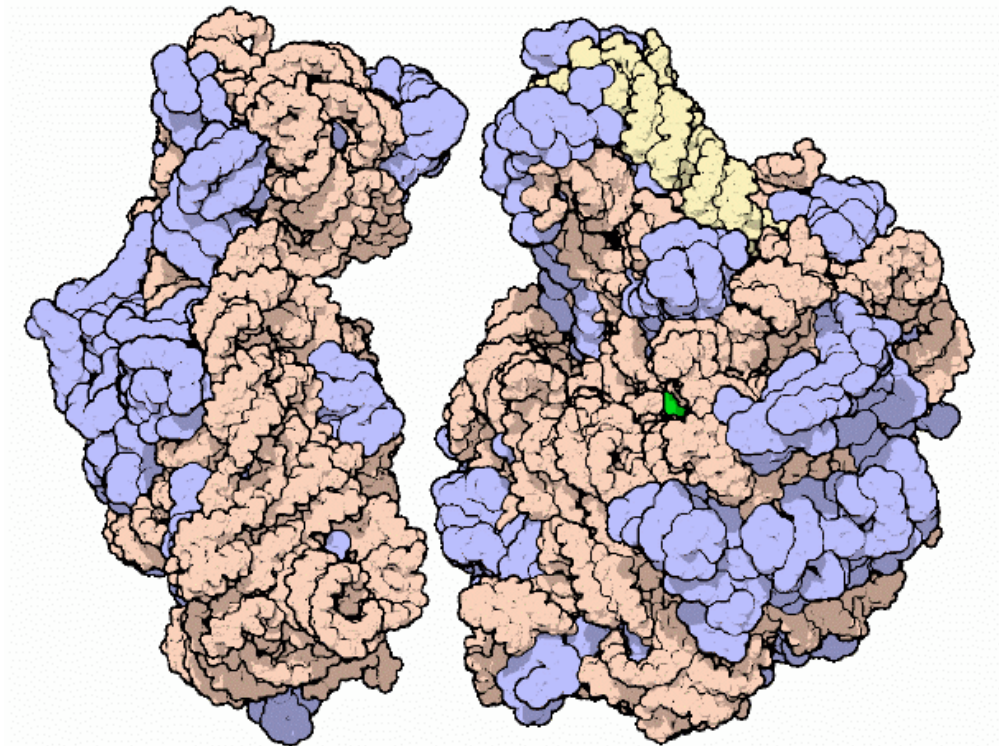
The large subunit contains the active site of peptide synthesis (near green adenine) and two RNA chains (23S orange and 5S yellow) and dozens of proteins (some of which are missing in X-ray structures).

1ffk (Moore/Steitz)

The first complete ribosome subunit structures (1fjg, 1ffk, and 1fka), determined almost a decade ago, ushered structural biology into a new era. Since that time, more than 120 ribosome structures consisting of 50S, 30S subunits, and complete 70S ribosomes have been determined. Structures — complexed with and without antibiotics, tRNAs, mRNAs, initiation factors, and release factors — provide a basis for understanding how the ribosome works and are useful tools for drug development.

PDB Molecule of the Month October 2000; PDB news October 2009

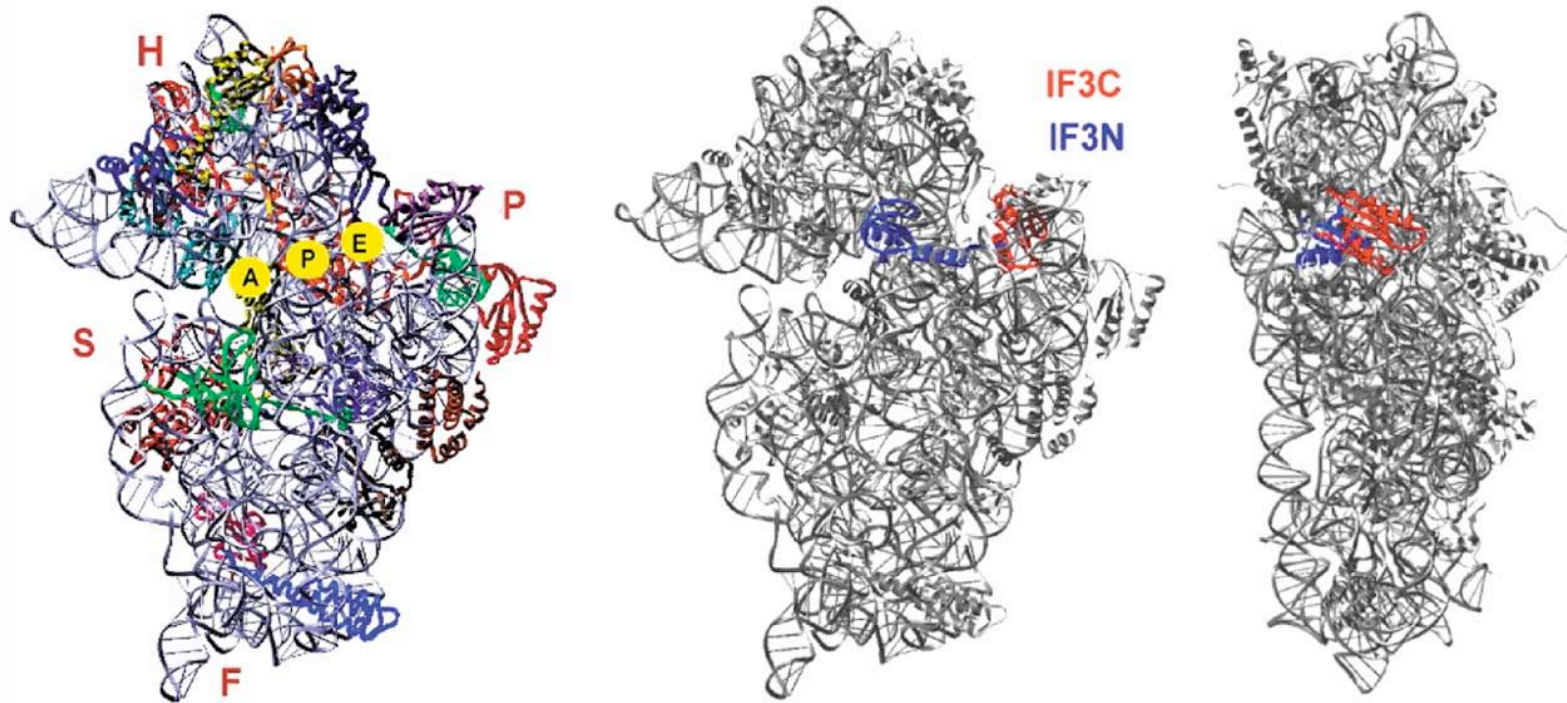Proteins and RNA comprising the small subunit (PDB_ID 1fka)
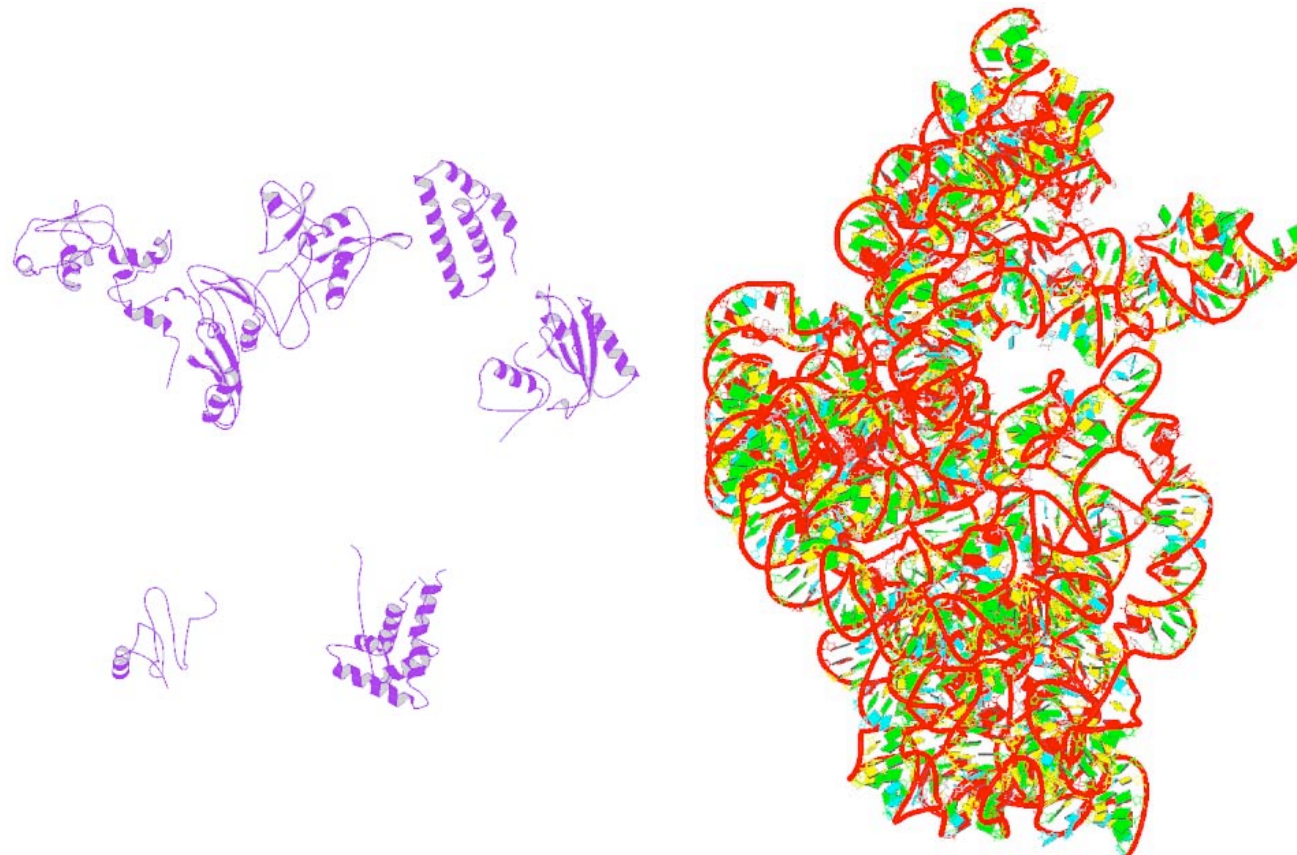
Proteins and RNA comprising the large subunit (PDB_ID 1ffk)
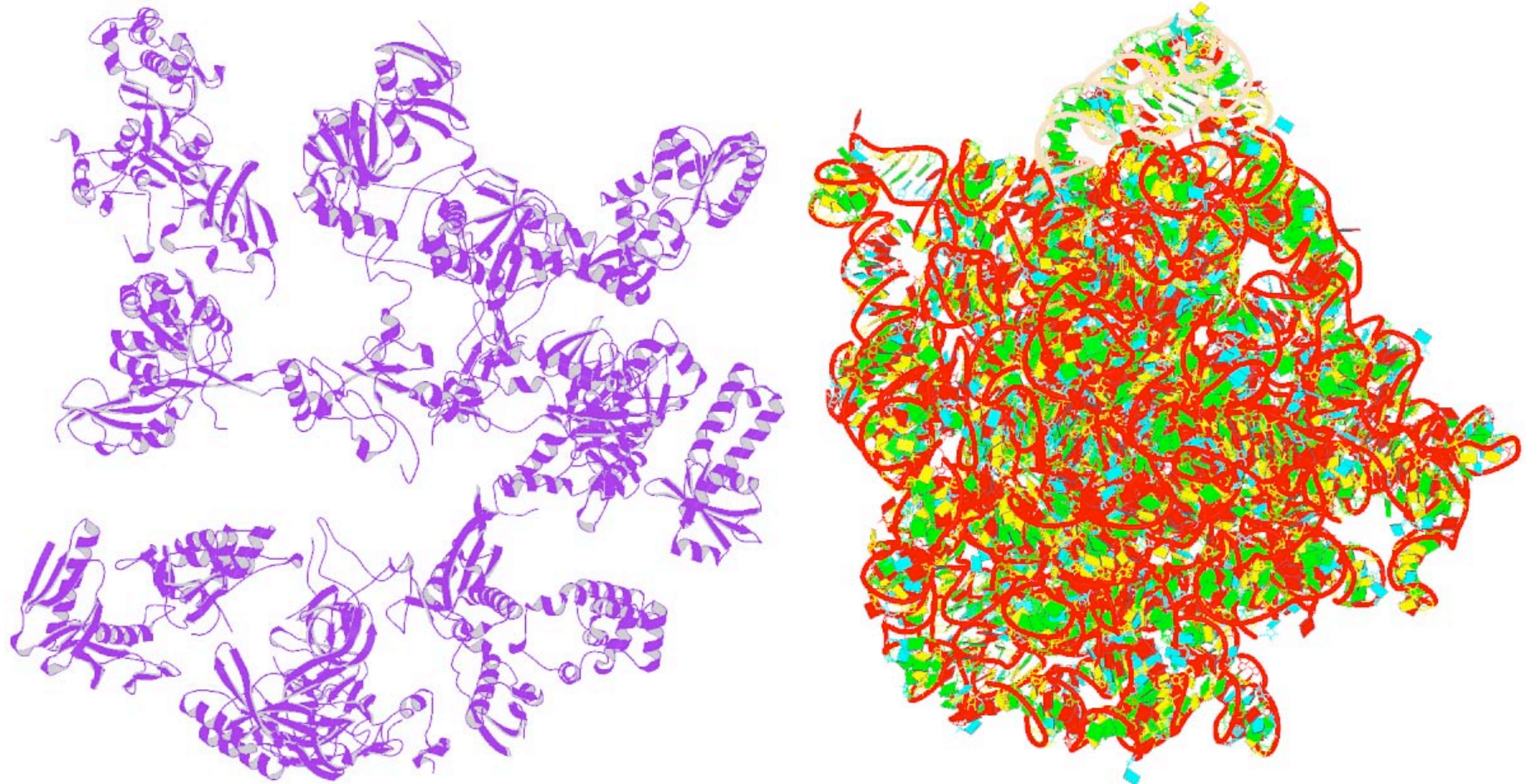
Small ribosomal subunit

Small subunit seen from the interface side (side facing large subunit in 70S ribosome).

RNA shown as simple ribbons (silver) and proteins in different colors. Major subdivisions labeled: H, head; S, shoulder; P, platform; F, foot. Approximate locations of A-, P-, and E-tRNA-binding sites marked. Middle: same view as that on left, but entire subunit gray. Location of IF3 marked in red (for C-terminal domain, IF3C) and blue (N-terminal domain, IF3N, and intersubunit linker). Right: Side view of small subunit, with its platform pointing toward the reader (obtained by 90° rotation about long axis of left and middle views). IF3 - an initiation factor that influences the binding of the other ligands and acts as a fidelity factor by destabilizing noncanonical codon-anticodon interactions.
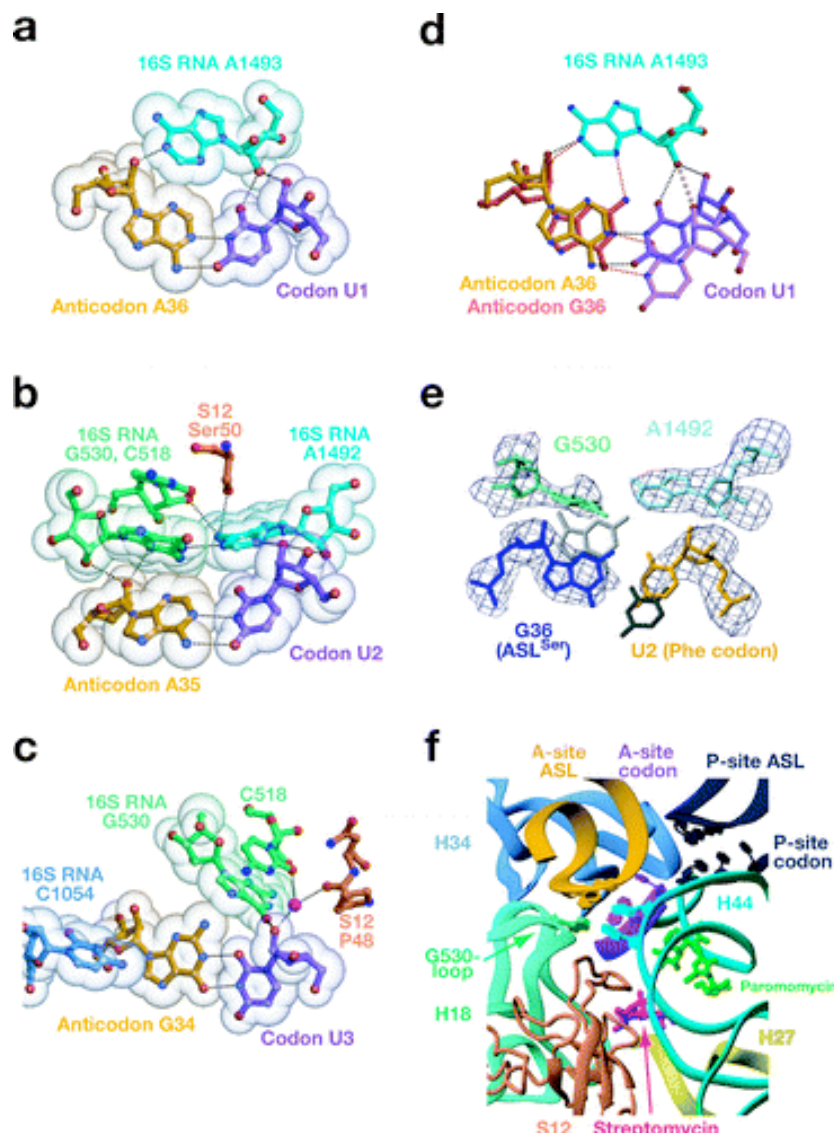
A. Yonath. (2002) "The search and its outcome: high-resolution structures of ribosomal particles from mesophilic, thermophilic, and halophilic bacteria at various functional states." *Ann. Rev. Biophys. Biomol. Struct.* 31, 257-273.

Kinetic proofreading hypothesis

(a) Two-step kinetic proofreading scheme applied to the ribosome. Here, R represents the ribosome, S the aa tRNA complexed with EF-Tu (elongation factor Tu), and S* the aa tRNA alone. P represents the tRNA after peptide bond formation. Overall selectivity enhanced because tRNA must pass unidirectionally and without dissociating through both selection steps in order to take part in protein synthesis..
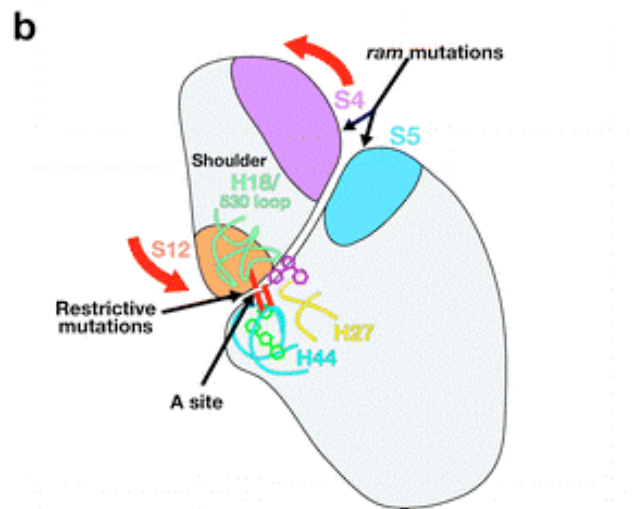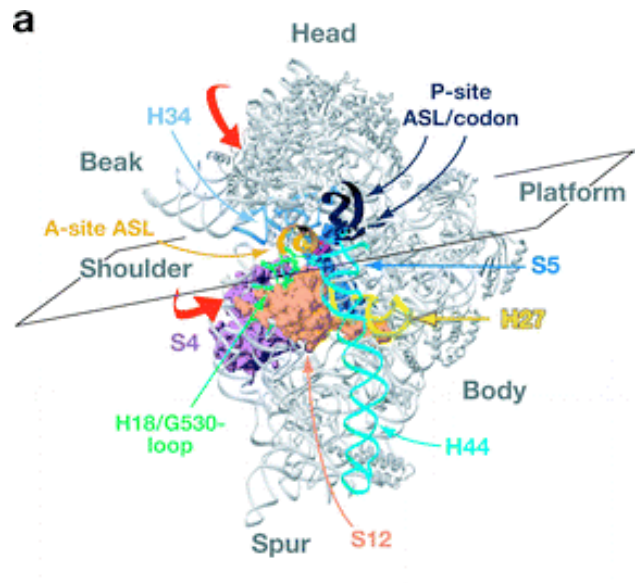
J.M. Ogle & V. Ramakrishnan. (2005) "Structural insights into translational fidelity." *Ann. Rev. Biochem.* 74, 129-177.

Recognition of the codon-anticodon helix by the ribosome

(a–c) the 1st to 3rd base pairs between a UUU codon and the cognate GAA anticodon from the Phe anticodon stem-loop (ASL). Ribosomal elements closely interact with the minor groove at the first two bps but less so at the 3rd (wobble) bp. (d) Interactions at a UG mismatch from a Leu near-cognate ASL at the 1st codon position. The cognate UA base pair is shown for comparison. (e) UG mismatch from a Ser near-cognate ASL, showing Watson-Crick geometry and implying an unusual tautomer for U or G. The electron density and alternatives for U or G representing their putative locations if the UG pair had standard wobble geometry and either U or G were positioned in the electron density.
(f) Ribosomal environment at the decoding center with codon, cognate ASL, and paromomycin. Three bases G530 (turquoise), A1492, and A1493 (cyan) line the minor groove of the codon-anticodon helix at the center of the figure.

J.M. Ogle & V. Ramakrishnan. (2005) "Structural insights into translational fidelity."
*Ann. Rev. Biochem.* 74, 129-177.

# Domain closure in the 30S subunit induced by cognate tRNA binding (red arrow)

(a) Overview of 30S elements involved in decoding.

(b) A schematic diagram illustrating the relationship between domain closure (shoulder movement) and elements in the 30S subunit that affect translational fidelity. The view shows a cross section through the 30S subunit indicated by the plane in (a).

J.M. Ogle & V. Ramakrishnan. (2005) "Structural insights into translational fidelity." Ann. Rev. Biochem. 74, 129-177.

EM shows that tRNA is significantly distorted in the kirromycin-stalled complex compared to the crystal structure of the ternary complex
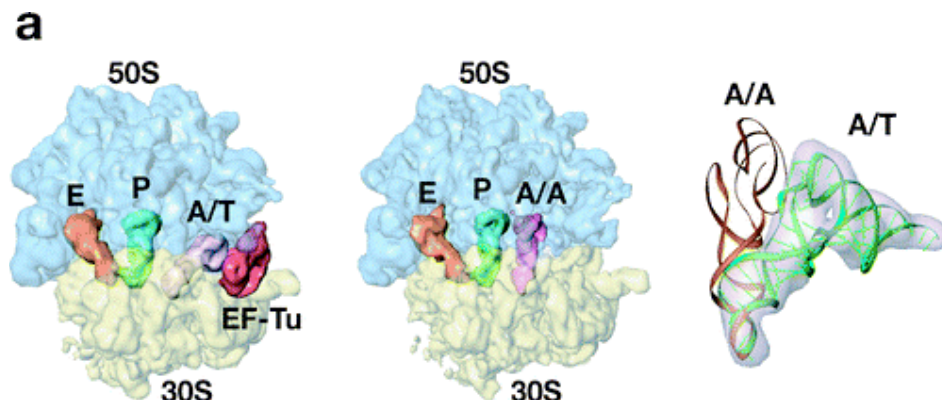

(a) Overviews of cryo-EM structures of the ribosome with E- and P-site tRNAs and with ternary complex (left) or accommodated A-site tRNA (center), and density showing a better fit for bent rather than straight tRNA in the ternary complex bound to the ribosome (right). Reproduced with permission from (146).
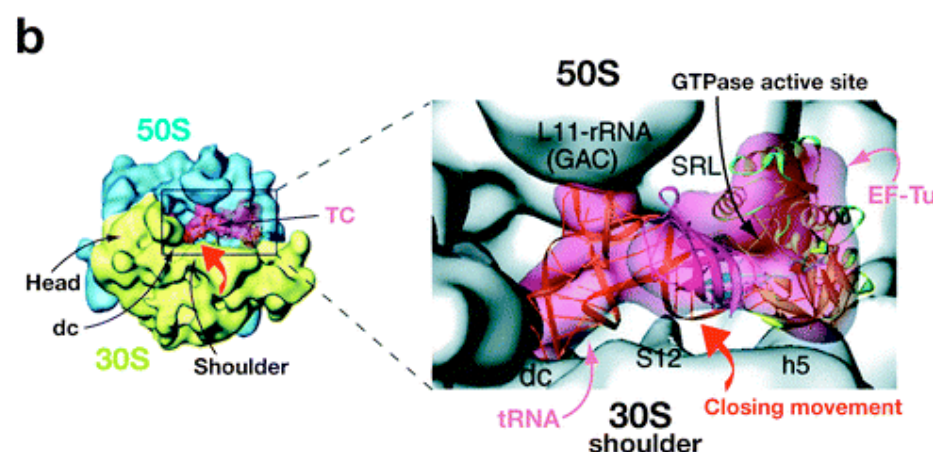
(b) Details of the environment of the ternary complex, in the context of the 30S domain closure, indicated by the red arrow.

# Structure of the ternary complex of EF-Tu, tRNA, and a GTP analog
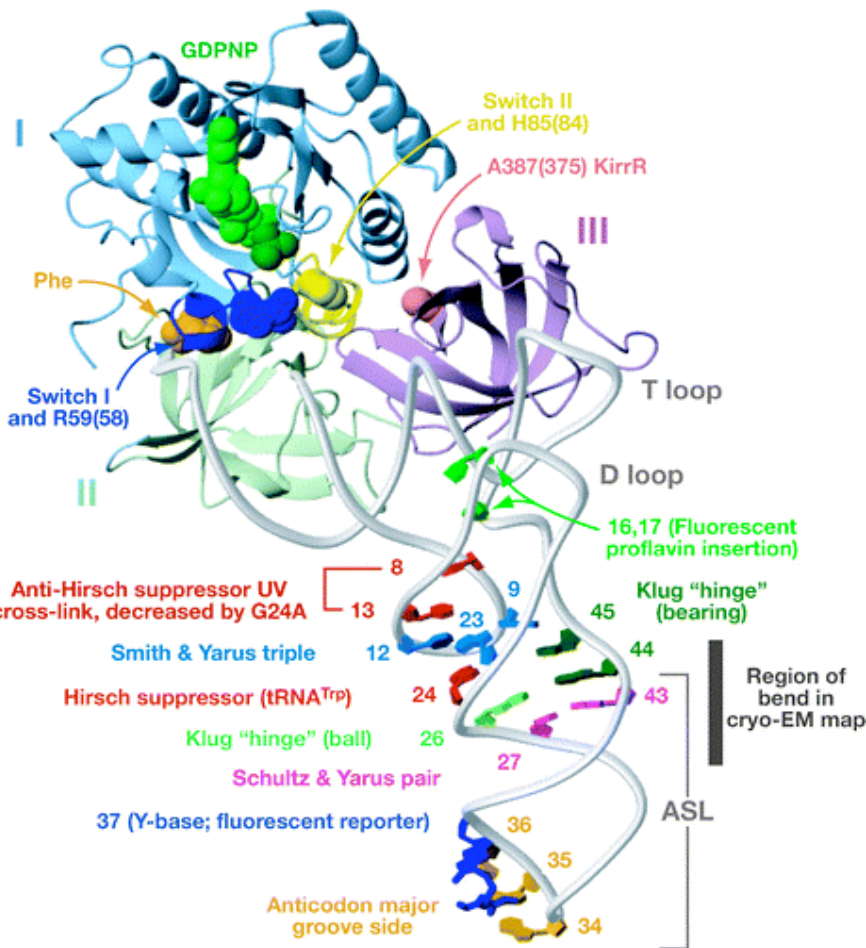
Elements of tRNA and EF-Tu that are known or likely to be involved in translational fidelity or that were used as reporters are mapped onto the structure.

J.M. Ogle & V. Ramakrishnan. (2005) "Structural insights into translational fidelity."
Ann. Rev. Biochem. 74, 129-177.

Making sense of the 30S subunit structure

Masayasu Nomura assembly map for the 30S subunit
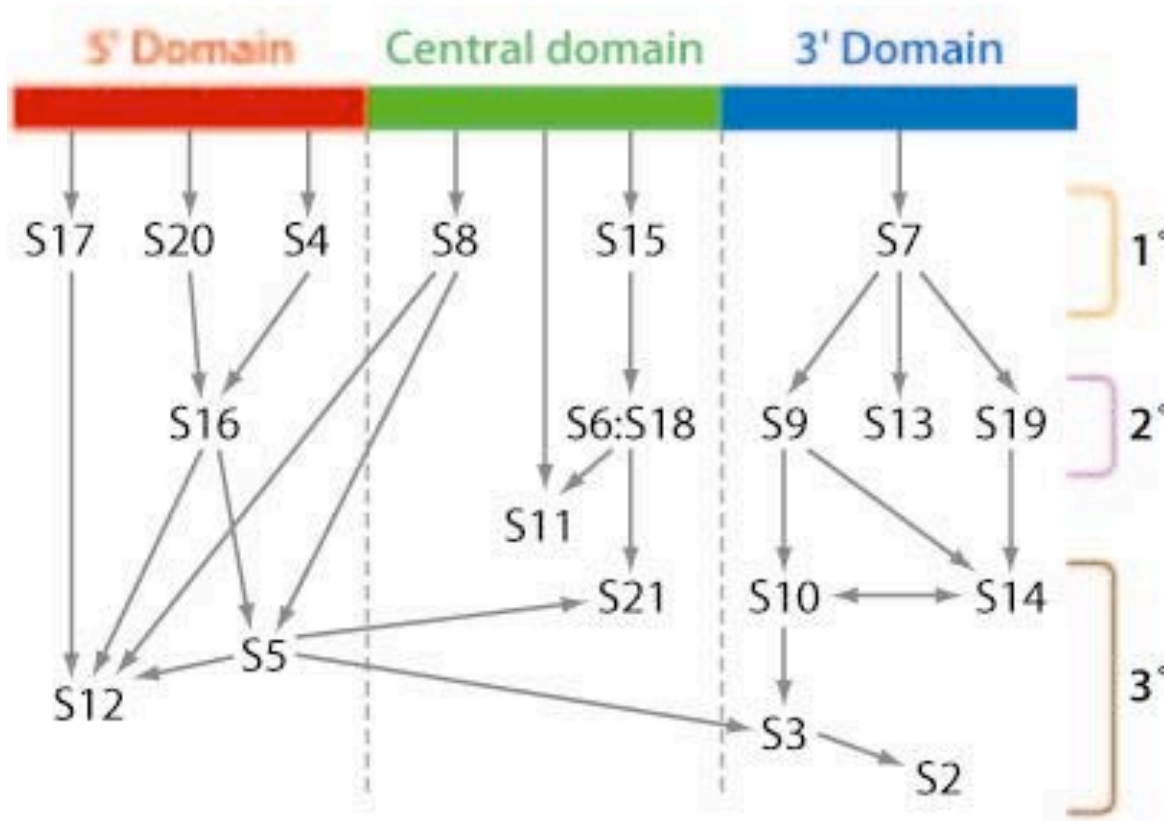
Traditional Nomura assembly map of rRNA reorganized according to domains, with arrows indicating the facilitating effect of binding between proteins. Proteins categorized as 5′, central, or 3′ domain proteins, and either primary (1°), secondary (2°), or tertiary (3°) binding proteins, the last two of which depend upon proteins from the previous category for binding to 16S rRNAs.

M.T. Sykes & J.R. Williamson. (2009) "A complex assembly landscape for the 30S ribosomal subunit." *Ann Rev. Biophys.* 38, 197-215.

Comparison of different representations of the 30S subunit
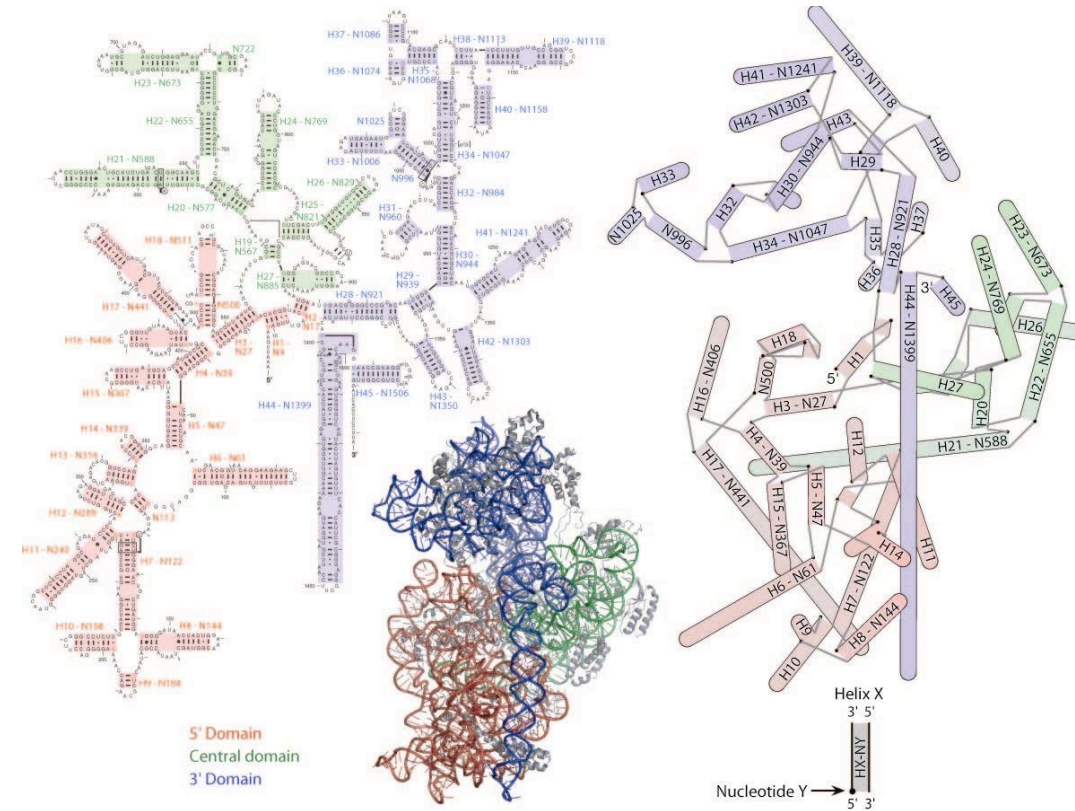
(a) Traditional 2° structure diagram of 16S rRNA. (b) 3D image of the 30S subunit including proteins (gray). (c) 2D projection of the 16S rRNA helices calculated such that the layout is faithful to the 3D structure. Helices shown as cylinders, capped by a semicircle when helical strands are contiguous. Black dots denote first nucleotide of helices, and gray lines denote connecting strands between helices. Helices shaded in hybrid according to position along the axis normal to the page (darker colors more distant). Hybrid representation blends the simplicity of the 2° structure with 3D information and captures the overall shape of the subunit.

M.T. Sykes & J.R. Williamson. (2009) "A complex assembly landscape for the 30S ribosomal subunit." *Ann Rev. Biophys.* 38, 197-215.

Ribosomal protein-RNA contacts
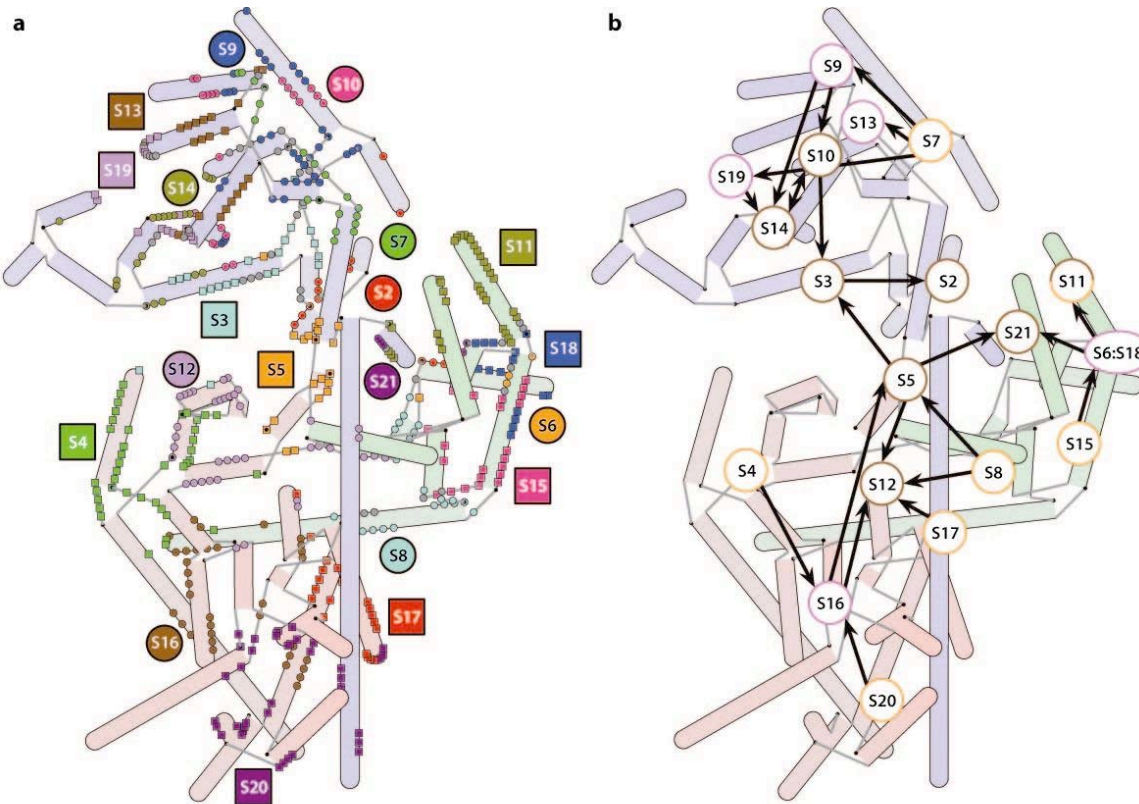
(a) Contacts mapped onto a hybrid 2D representation of 16S rRNA. Contact annotated when any non-hydrogen atoms from a nucleotide and an amino acid residue lie within 4 Å of each other. Cases in which a single nucleotide contacts multiple proteins noted in gray. Protein labels placed near the primary sites of contact. (b) Nomura map overlaid on a hybrid schematic representation of the 16S rRNA. Labels for proteins are located according to their approximate position in the 3D structure of the 30S subunit. Primary binding proteins appear to bind in the periphery of the 30S subunit, and tertiary proteins around the cleft containing the decoding site.

M.T. Sykes & J.R. Williamson. (2009) "A complex assembly landscape for the 30S ribosomal subunit." *Ann Rev. Biophys.* 38, 197-215.

Hybrid representations of 16S rRNA annotated with information about changes in accessibility to chemical modification during steps in 30S subunit assembly.
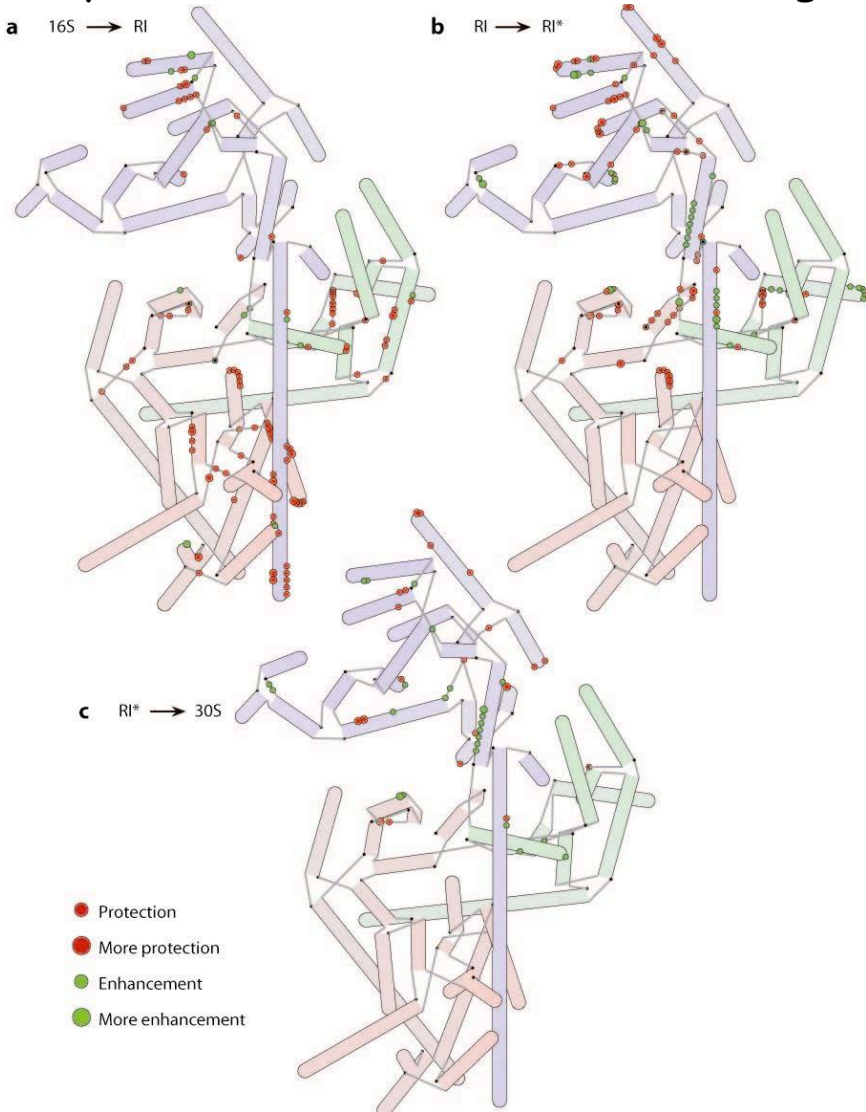

Extent of decreased accessibility (protection) or increased accessibility (enhancement) indicated by size of circles used to annotate nucleotides. (a) Changes during formation of a reconstitution intermediate (RI). (b) Changes during RI to RI* transition. (c) Changes while complete 30S subunit is formed from RI*. The RI to RI* transition enhancements to modification are suggestive of a large refolding of the RNA that exposes several nucleotides.

M.T. Sykes & J.R. Williamson. (2009) "A complex assembly landscape for the 30S ribosomal subunit." *Ann Rev. Biophys.* 38, 197-215.
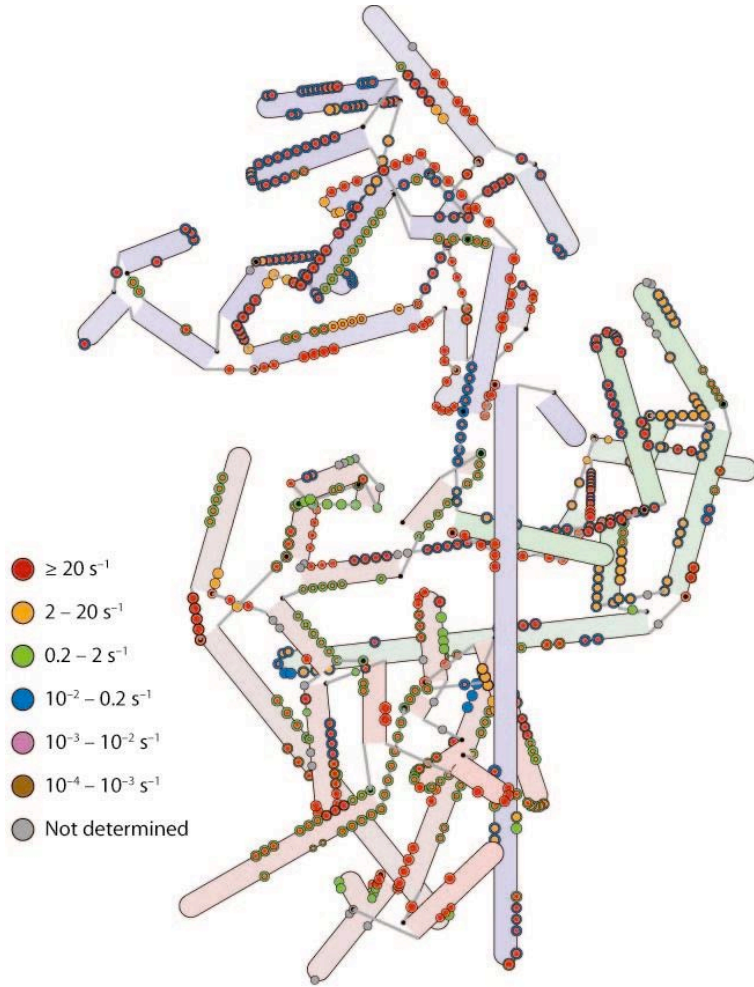
Hybrid representations of 16S rRNA annotated with with rate constants for protein binding determined by pulse-chase quantitative mass spec.
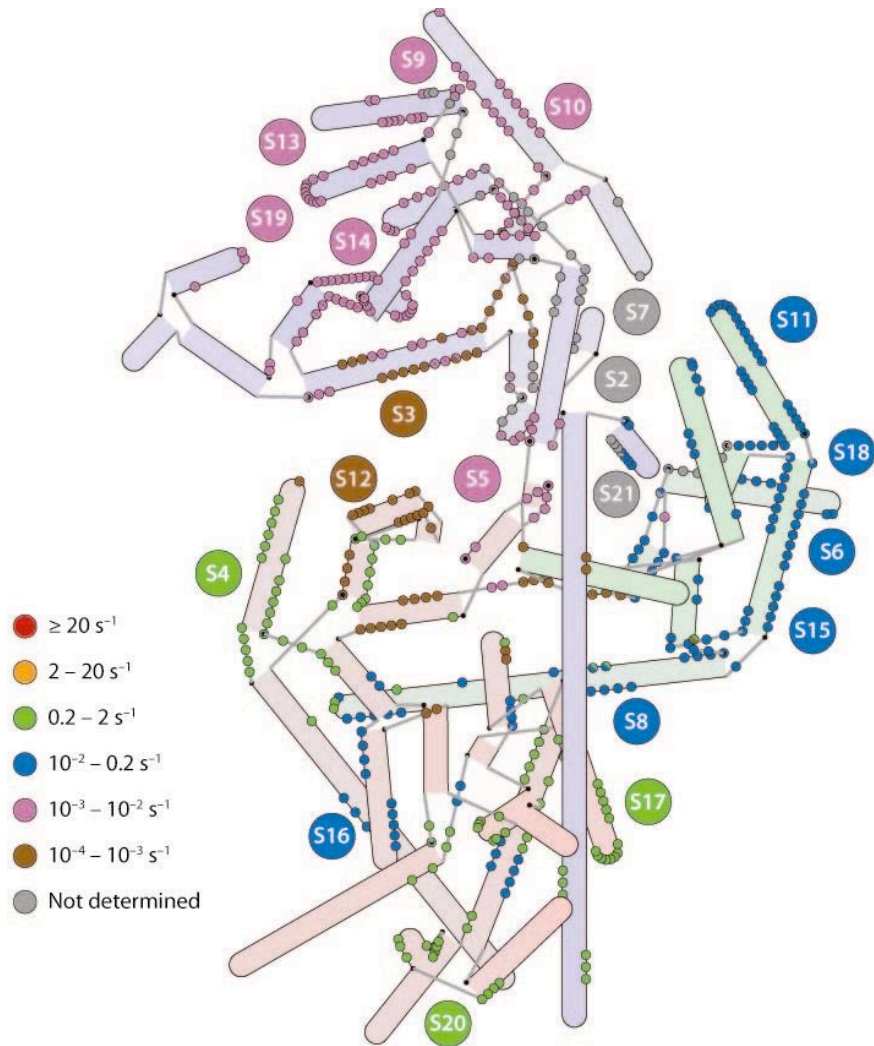
Nucleotides that make protein contacts color-coded according to the binding rate of the protein contactED. Cases in which two proteins are contacted by a single nucleotide noted by semicircles. Nucleotides that contact proteins S2, S7, and S21 marked in gray, as no rate constant data obtained for these proteins. Rates generally cluster by domain, with fastest rates observed in 5´-domain and slowest in 3´-domain, the exception being the 5´-domain protein S12, (indicated by the brown circles).

M.T. Sykes & J.R. Williamson. (2009) "A complex assembly landscape for the 30S ribosomal subunit." *Ann Rev. Biophys.* 38, 197-215.

Hybrid representations of 16S rRNA annotated with rate constants for protection from hydroxyl radical cleavage .

Legend:
- ≥ 20 s⁻¹ $\geq 20\ s^{-1}$
- 2 – 20 s⁻¹ $2-20\ s^{-1}$
- 0.2 – 2 s⁻¹ $0.2-2\ s^{-1}$
- $10^{-2}-0.2\ s^{-1}$
- $10^{-3}-10^{-2}\ s^{-1}$
- $10^{-4}-10^{-3}\ s^{-1}$
- Not determined

In cases in which two rate constants are calculated for two phases of protection, concentric circles are displayed, with the inner circle colored according to the rate constant of the initial burst of protection and the outer circle colored according to the second, slower protection. Area displayed is proportional to the amplitude of the protection (smaller amplitudes noted by smaller circles). Fast rates across the entire 16S suggest multiple nucleation sites for assembly. Whereas initial burst rates are generally faster than rates observed for protein binding, the second slower rates are on par with those observed for protein binding in many cases.

M.T. Sykes & J.R. Williamson. (2009) "A complex assembly landscape for the 30S ribosomal subunit." *Ann Rev. Biophys.* 38, 197-215.

Large ribosomal subunit

Appearance of the large ribosomal subunit from *H. marismortui* in electron density maps at different resolution
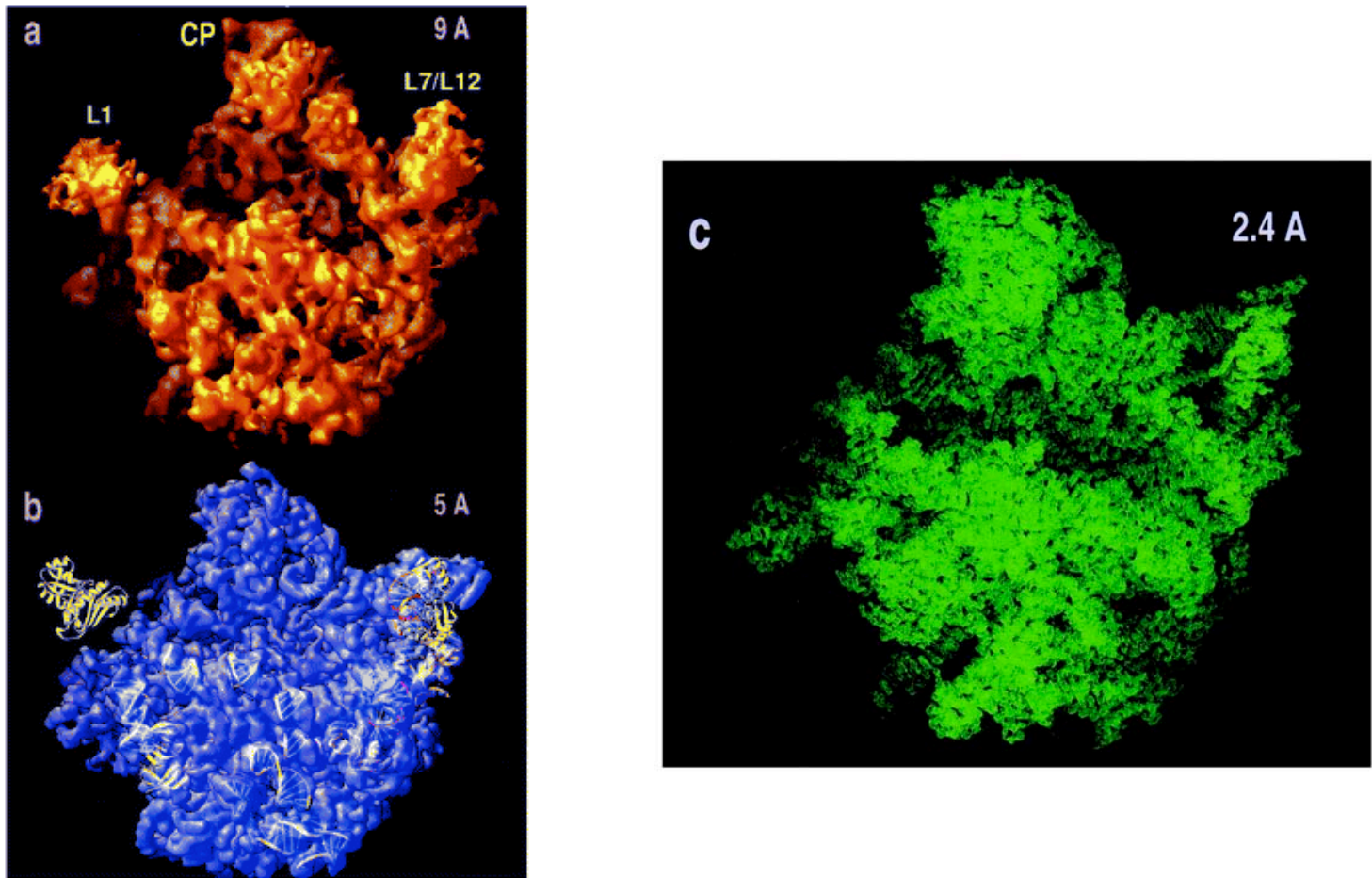
Subunit shown in crown view at (a) 9 Å, (b) 5 Å, and (c) 2.4 Å resolution. CP designates the central protuberance. The L1 stalk, visible at low resolution, disappears as resolution improves.

Structure of kink-turn 7 in the 23s rRNA of the *H. marismortui* ribosome
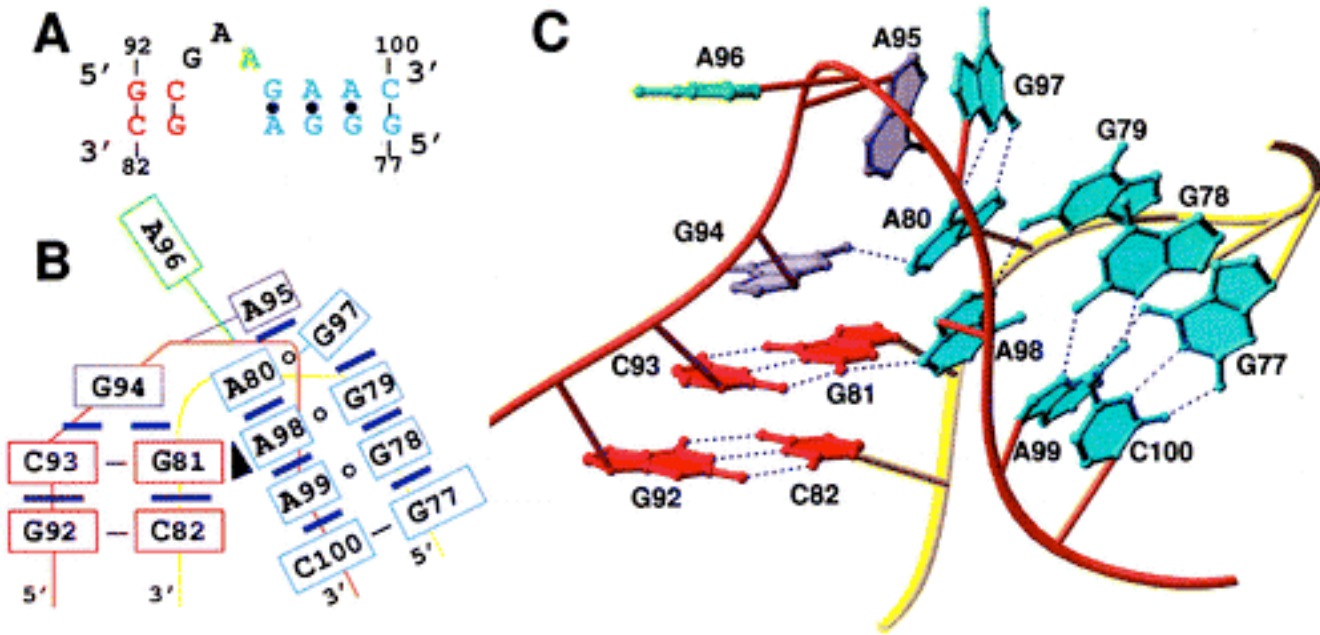
(a) 2° structure of kink turn-7. C-stem - red; NC-stem - blue; bulged nucleotide - green. (b) Base pairing and stacking interactions in kink turn-7. Black triangle - A-minor interaction. (c) kink turn-7 in 3D. Backbone of kinked strand - orange; unkinked strand - yellow. Dashed lines - H bonds

A-minor motifs in the 23s rRNA of the *H. marismortui* ribosome
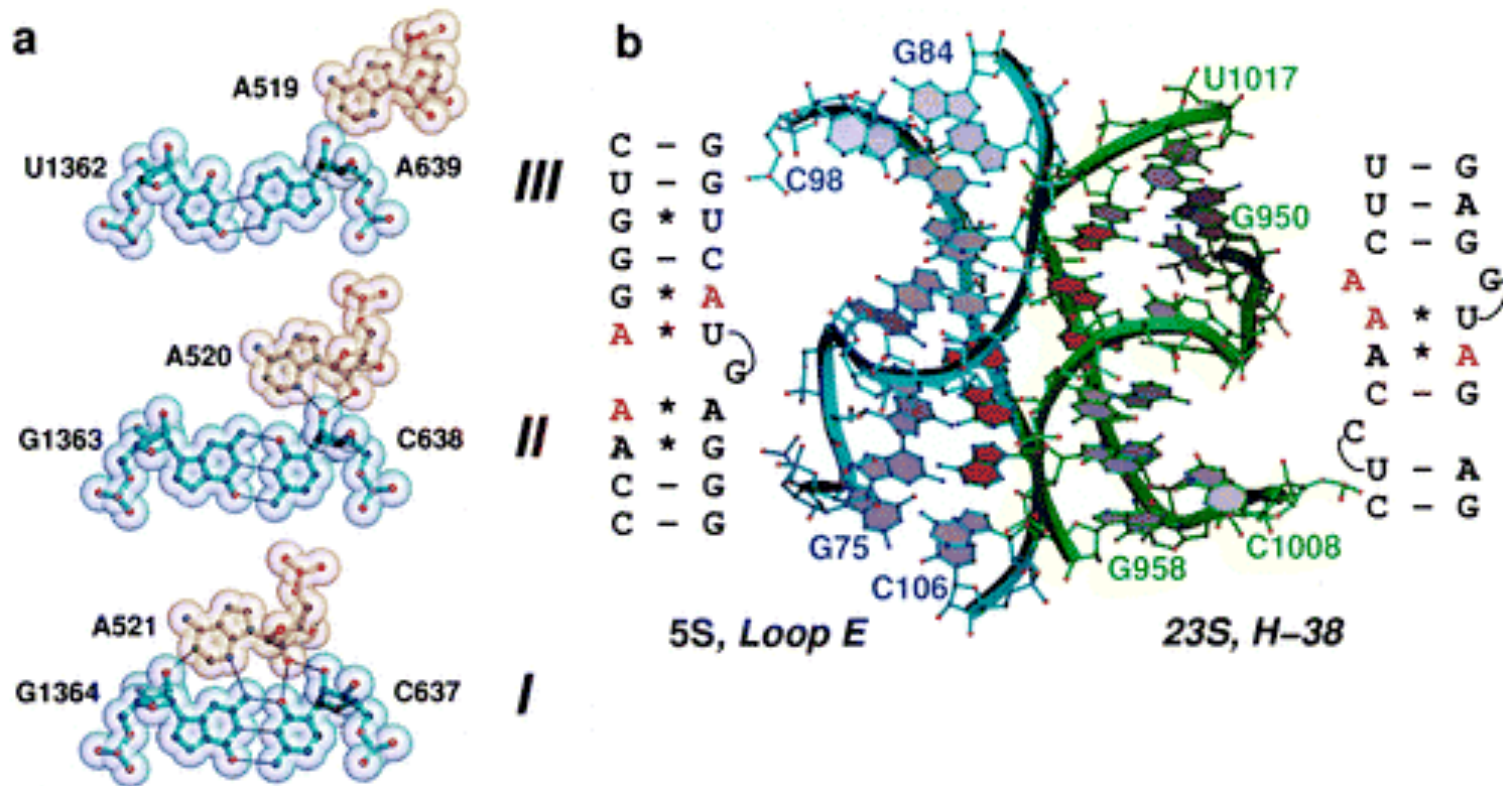
(a) Examples of the three most important kinds of A-minor motifs from the *H. marismortui* 23S rRNA. Types I and II are A-specific. Type III may involve other bases, but A is preferred.
(b) Interaction between helix 38 of 23S rRNA and 5S rRNA. The only direct contacts between these two molecules are six A-minor interactions, involving three As in 23S rRNA and 3 As in 5S rRNA that are symmetrically disposed. Secondary structure diagrams are provided for the interacting sequences

P.B. Moore & T.A. Steitz. (2003) "The structural basis of large ribosomal subunit function."
*Ann Rev. Biochem.* 72, 813-850.

Space-filling model of *H. marismortui* large ribosomal subunit with a transition state analog bound (view down active site cleft).
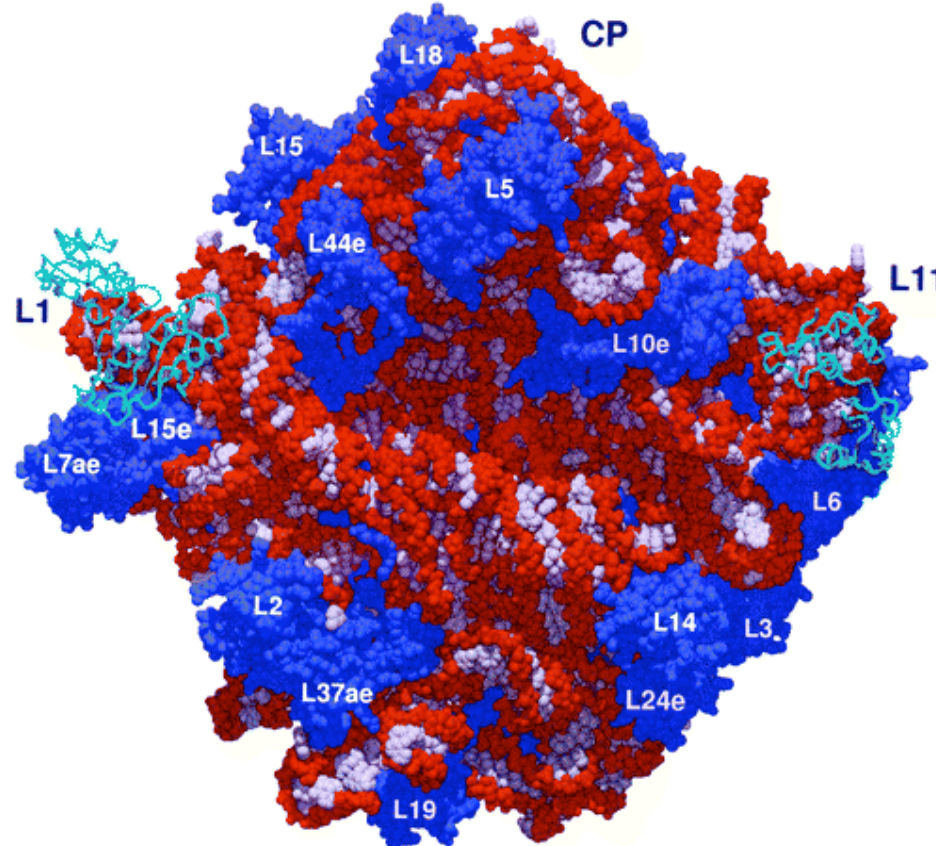
Bases - white, sugar-phosphate backbone - orange, substrate analog (in center) - red. Proteins whose structures are defined by the 2.4 Å resolution map - blue. Cyan ribbon - proteins whose structures are independently determined and positioned approximately using lower resolution electron densities. Identification numbers provided for all proteins. CP - the central protuberance.

P.B. Moore & T.A. Steitz. (2003) "The structural basis of large ribosomal subunit function."
*Ann Rev. Biochem.* 72, 813-850.

Ribosomal proteins in the *H. marismortui* large ribosomal subunit
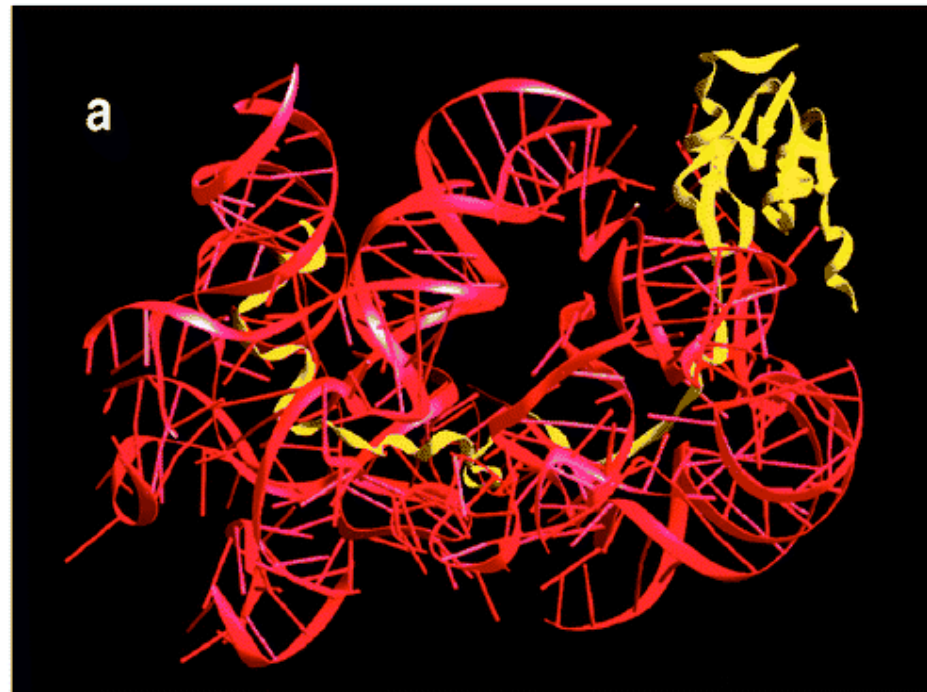
Ribbon representation of L15 (yellow) and the RNA sequences with which it interacts (red). Globular domain of protein is to solvent on surface of ribosome, but extended tail penetrates deeply into subunit.

P.B. Moore & T.A. Steitz. (2003) "The structural basis of large ribosomal subunit function."
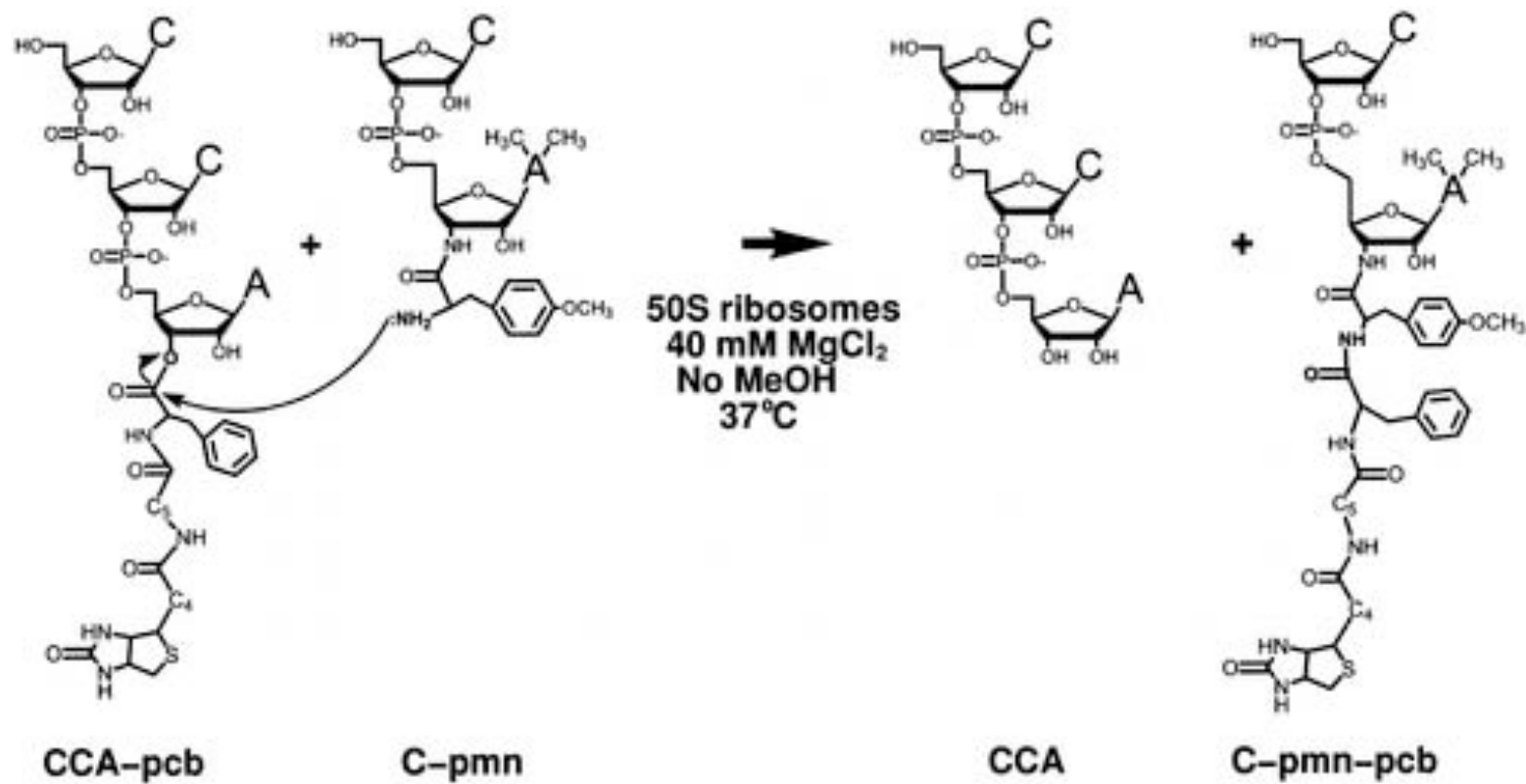*Ann Rev. Biochem.* 72, 813-850.

Ribosomal proteins in the *H. marismortui* large ribosomal subunit
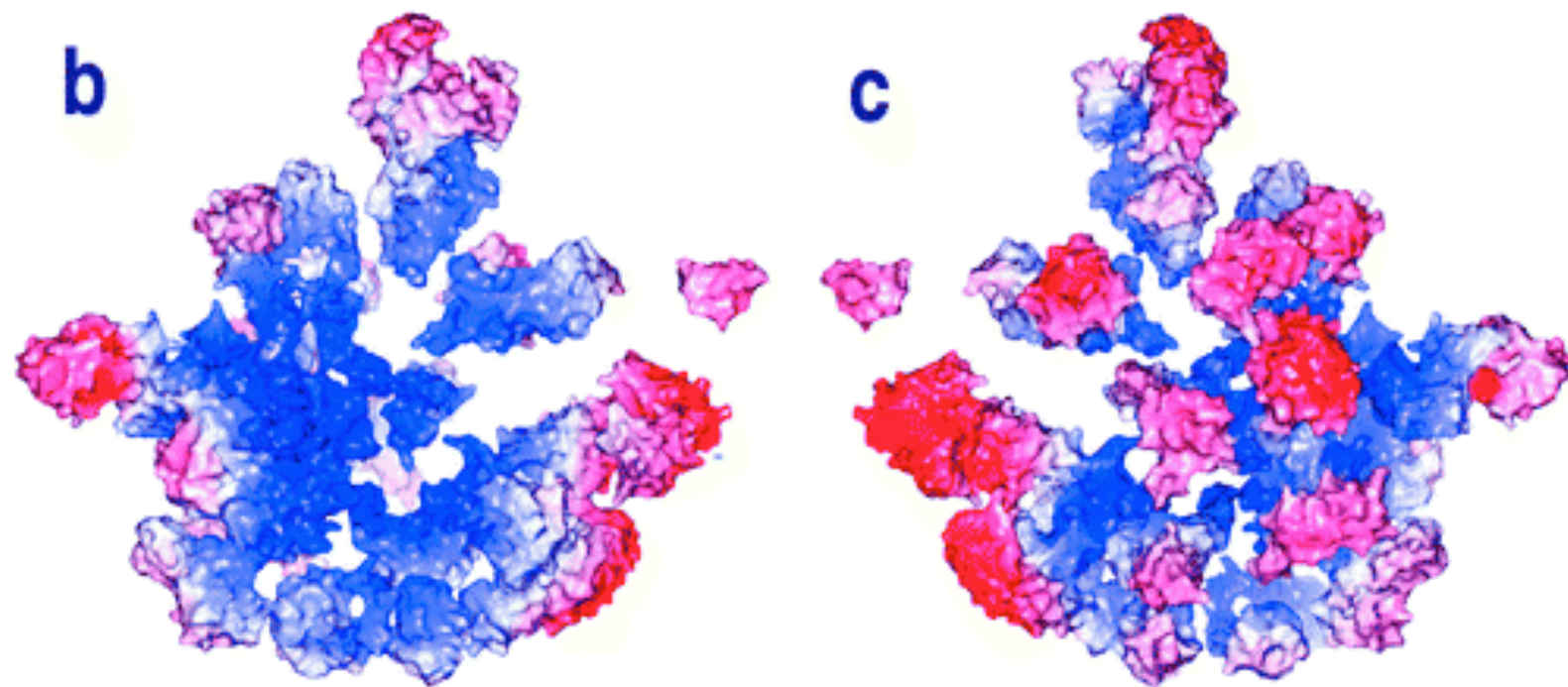
Space-filling representation of proteins in *H. marismortui* large ribosomal subunit, with RNA removed, and color-coded to display electrostatic charge potential: negative - red; positive - blue; neutral - white. Crown view in (b), and rotated 180° about vertical axis in (c). Surface of the globular domains that face exterior are acidic, but those that face interior, including their tails, are basic

P.B. Moore & T.A. Steitz. (2003) "The structural basis of large ribosomal subunit function."
*Ann Rev. Biochem.* 72, 813-850.

Ribosome-catalyzed peptide bond-forming reaction involving low mol wt substrates

Reaction of CCA-Phe-caproic acid-biotin (CCA-pcb) and C-puromycin (C-pmn) that yields CCA and C-puromycin-Phe-caproic acid-biotin (C-pmn-pcb) catalyzed by large ribosomal subunits. Reactions of this type are analogous to the peptidyl transferase reaction, which occurs *in vivo* and is referred to as the "fragment reaction," because its substrates resemble the 3´ - termini of aminoacyl and peptidyl tRNAs

P.B. Moore & T.A. Steitz. (2003) "The structural basis of large ribosomal subunit function."
*Ann Rev. Biochem.* 72, 813-850.

Structure of the *H. marismortui* large ribosomal subunit with products of the fragment reaction bound in the peptidyl transferase center.
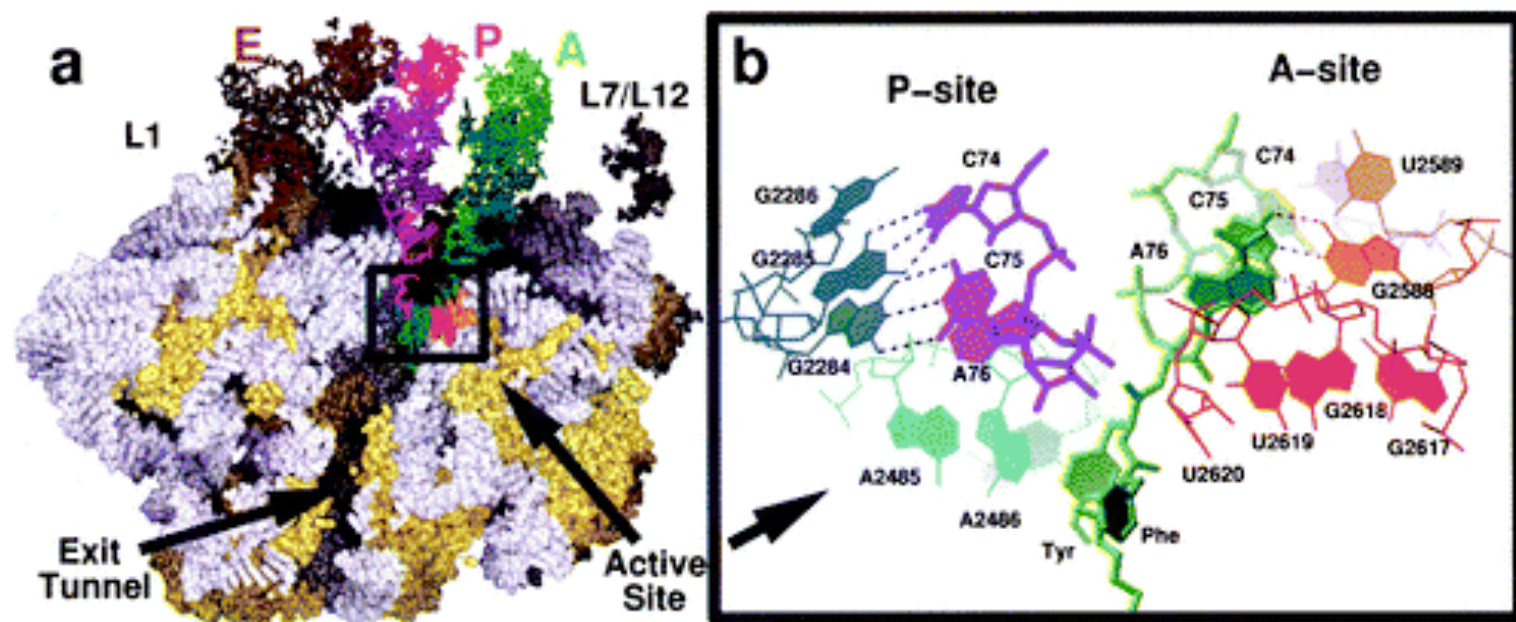
(a) Space-filling representation of complex with three intact tRNAs added in the positions tRNA assumes when bound to A, P, and E sites of the 70S ribosome. rRNA - white; ribosomal proteins - yellow. The subunit, which is oriented in the crown view, is cut in half along a plane that passes through the peptide exit tunnel, and front of structure removed to expose tunnel lumen. The active site area noted by box. (b) Close-up of the active site showing peptidyl product (green) bound to the A-loop (orange), and deacylated product (violet) bound to the P-loop (dark blue). N3 of A2486 (A2451 in *E. coli*) (light blue) is close to 3´-OH of the CCA, and base of U2620 (U2585) (red) has moved close to new peptide bond and 3´-OH of A76.

P.B. Moore & T.A. Steitz. (2003) "The structural basis of large ribosomal subunit function."
Ann Rev. Biochem. 72, 813-850.

Steps in the peptidyl transferase reaction pathway
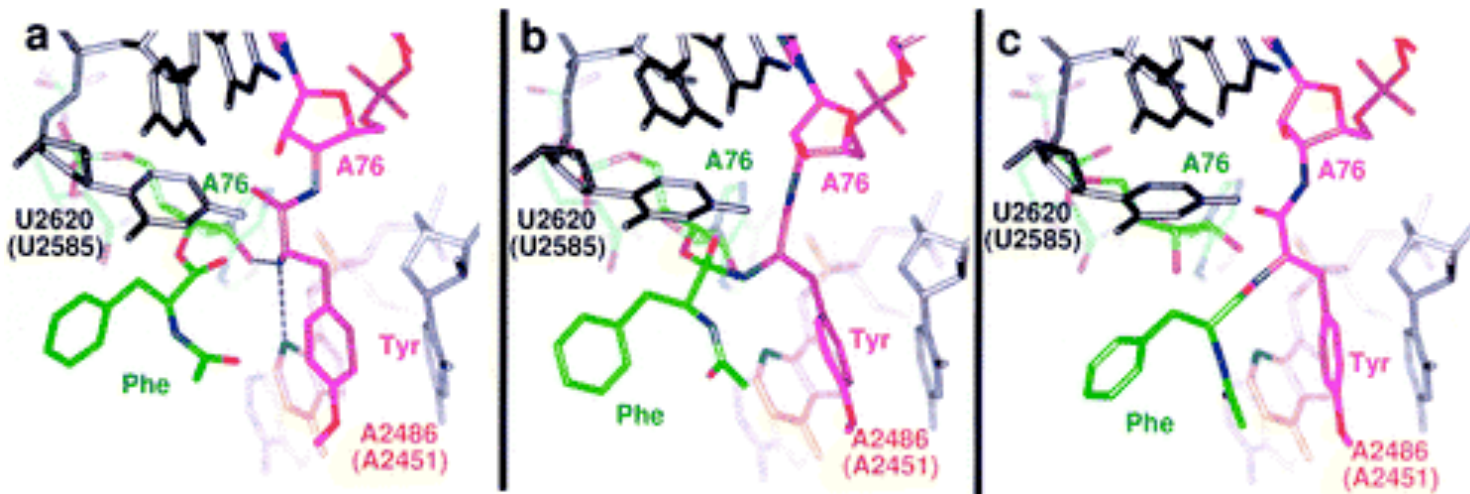
(a) Superposition of two independently determined cocrystal structures suggests that the α-amino group of an A-site substrate is positioned for a pro-R attack on the carbonyl carbon of the ester bond of the P-site substrate (green). (b) Model for tetrahedral intermediate that would result if reaction were to occur in manner suggested in (a). Note that the oxyanion points away from A2486 (2451). (c) Structure of products of peptidyl transferase reaction bound to peptidyl transferase center

P.B. Moore & T.A. Steitz. (2003) "The structural basis of large ribosomal subunit function." *Ann Rev. Biochem.* 72, 813-850.
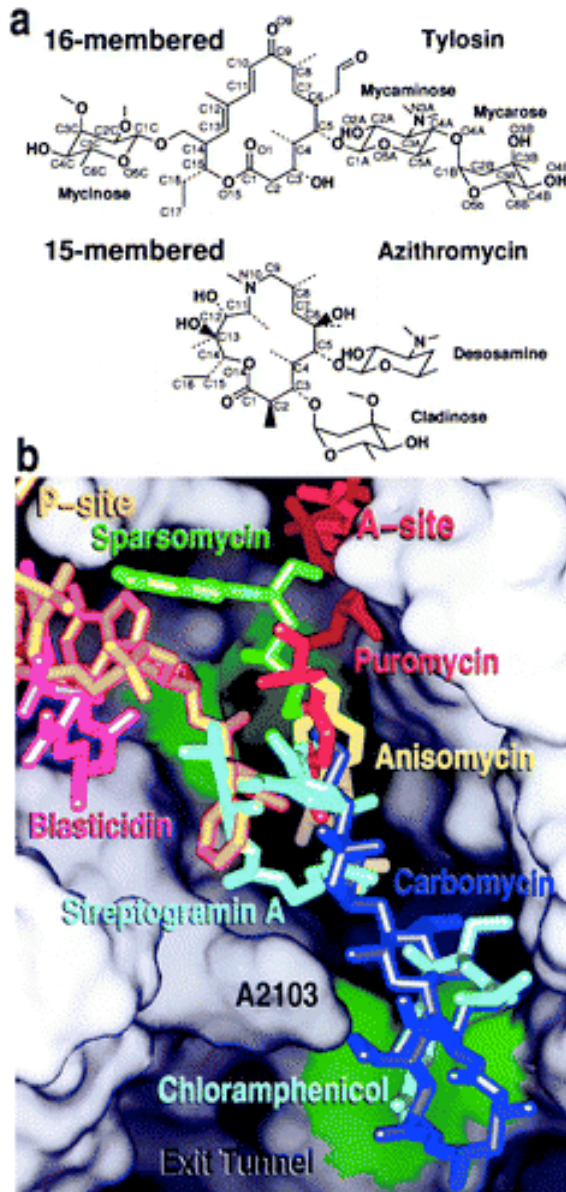
Interaction of macrolide antibiotics with the *H. marismortui* large ribosomal subunit.
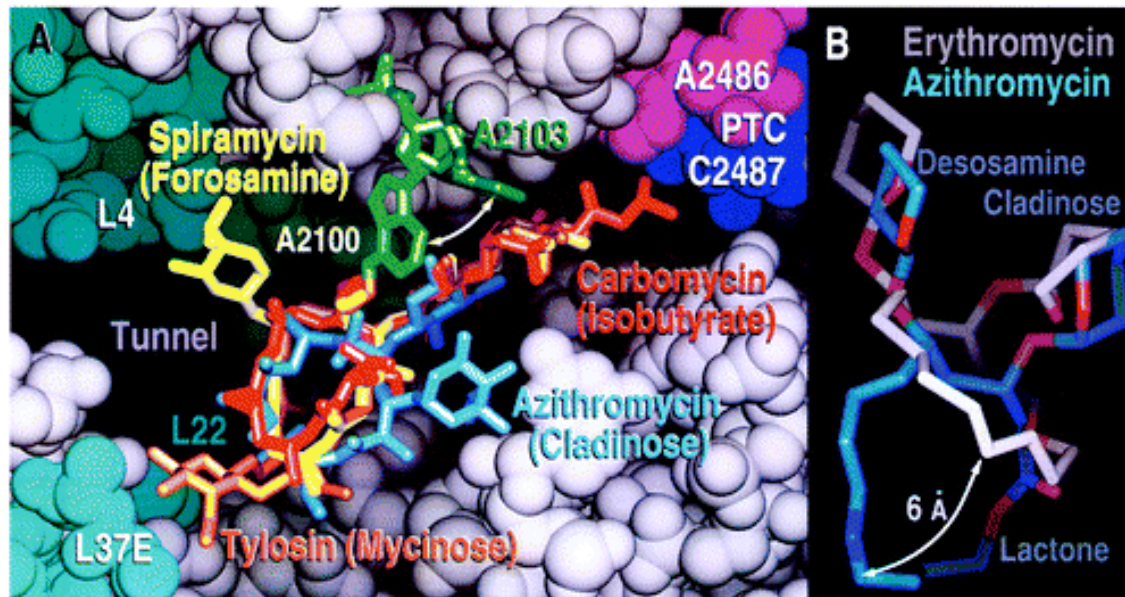
(a) Superposition of several macrolides/large ribosomal subunit complex structures containing: carbomycin (red); tylosin (orange); spiramycin (yellow); azithromycin (blue). The macrolide rings of the four antibiotics bind to virtually the same site in the proximal portion of the peptide exit tunnel. In the case of the 16-membered macrolides examined (tylosin, carbomycin, spiramycin), A2103 (2062) swings down so that its N6 can form a covalent bond with their aldehyde substituents. The differences between these drugs are due primarily to the substitutents on their macrolide rings, which differ in chemical nature, bulk, and placement. Some extend into the peptidyl transferase center. (b) Position assumed by erythromycin (white) when bound to the large ribosomal subunit from *D. radiodurans* compared to that adopted by azithromycin (blue) bound to the large ribosomal subunit from *H. marismortui*.

P.B. Moore & T.A. Steitz. (2003) "The structural basis of large ribosomal subunit function."
Ann Rev. Biochem. 72, 813-850.

# Antibiotic structures and antibiotic interactions with *H. marismortui* large subunit

(a) Structures of two macrolide antibiotics.

(b) Interactions of sparsomycin (green), puromycin (red), blasticidin S (magenta), chloramphenicol (light blue), carbomycin (dark blue), and streptogramin A (blue) with the large ribosomal subunit. The ribosome has been split open to reveal the lumen of the exit tunnel and adjacent regions of the peptidyl transferase site. Ribosomal components are depicted as a continuous surface. Seven independently determined cocrystal structures aligned by superimposing the 23S rRNA in each complex. The sites to which these antibiotics bind are all different, but there is extensive overlap.

P.B. Moore & T.A. Steitz. (2003) "The structural basis of large ribosomal subunit function."
Ann Rev. Biochem. 72, 813-850.

Conformational features of the 50S ribosomal subunit

The nucleotides in the large ribosomal unit adopt a wide variety of conformations.
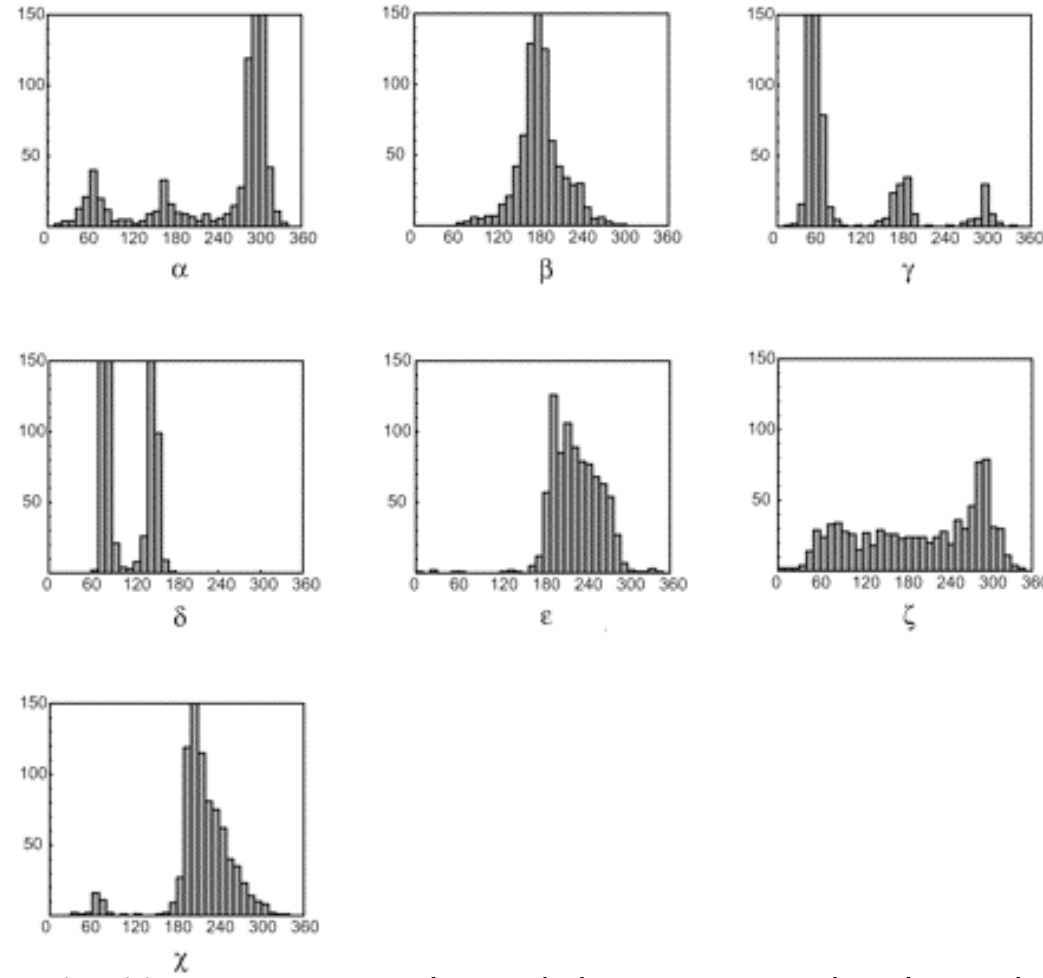
Histograms for the six backbone torsion angles and the torsion at the glycosidic bond in the 23S and 5S rRNA from the crystal structure of the 50S ribosomal subunit.

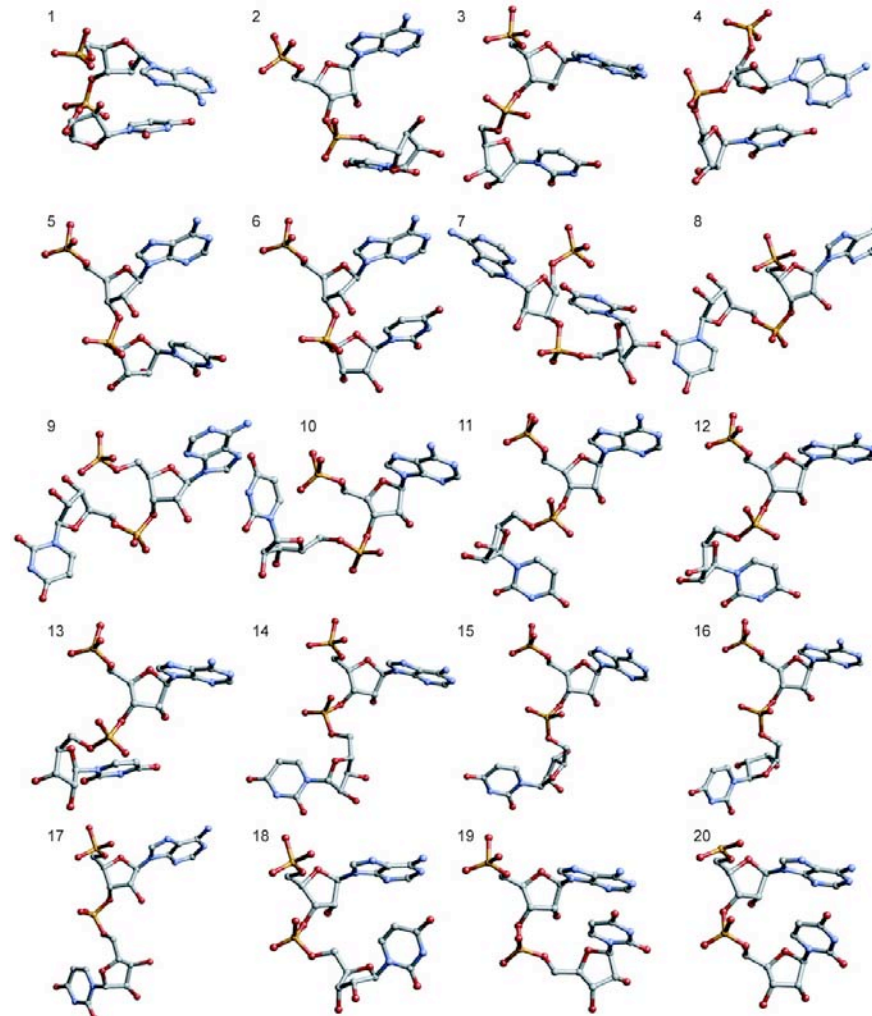Schneider et al. (2004) "RNA conformational classes." *Nucleic Acids Res.* 32, 1666-1677.

Stereo views of three RNA conformational families identified in the 50S subunit
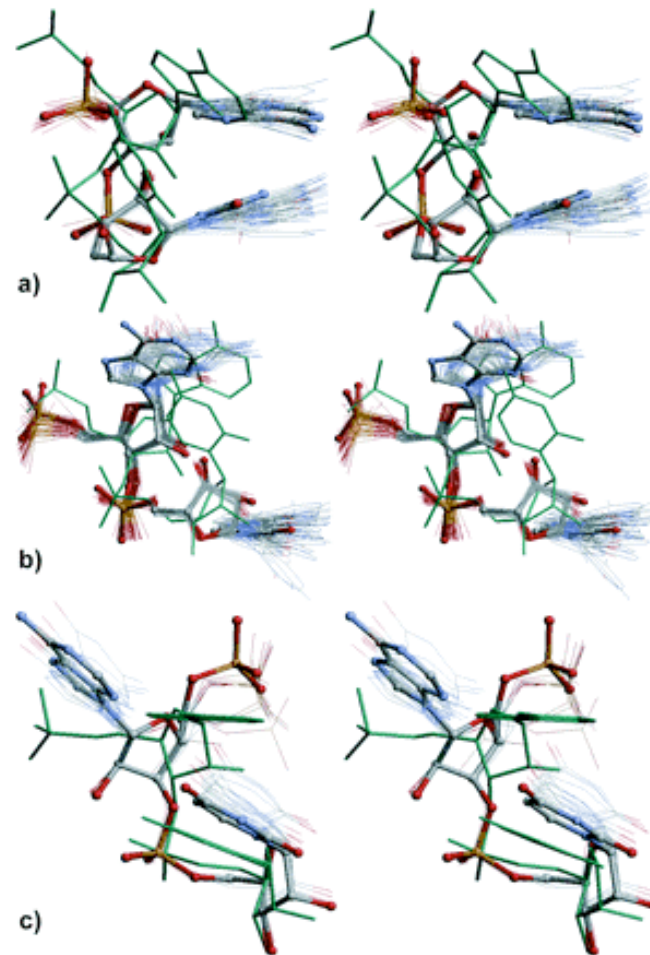
(a) Z-DNA-like backbone with both bases in *anti* orientation; (b) conformation seen in RNRN tetraloops; (c) conformation with parallel bases found in adenine platform. Overlaps of dinucleotides shown by thin lines. Representative average conformation shown as ball-and-stick model. Canonical A-RNA (pale green) superimposed on three average conformations.

Schneider et al. (2004) "RNA conformational classes." *Nucleic Acids Res.* 32, 1666-1677.

Gallery of the 19 RNA conformational families and the canonical A-RNA form (20) found in the large ribosomal subunit

Dinucleotides drawn with the 5´-end on top. All sequence 5´-AU-3´.

Schneider et al. (2004) "RNA conformational classes." *Nucleic Acids Res.* 32, 1666-1677.
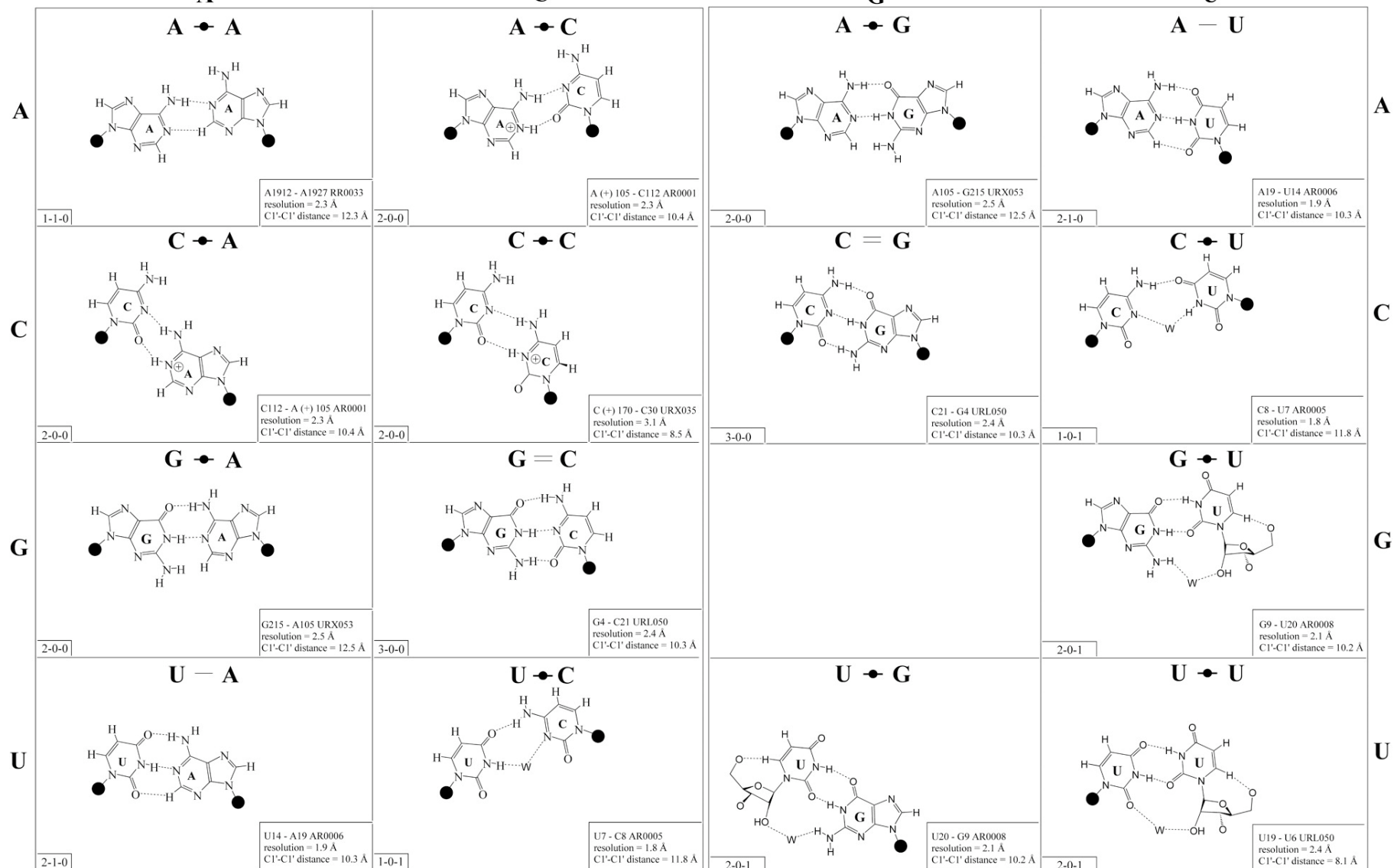
RNA base pairing

Identification of edges and orientations of RNA bases and base pairs
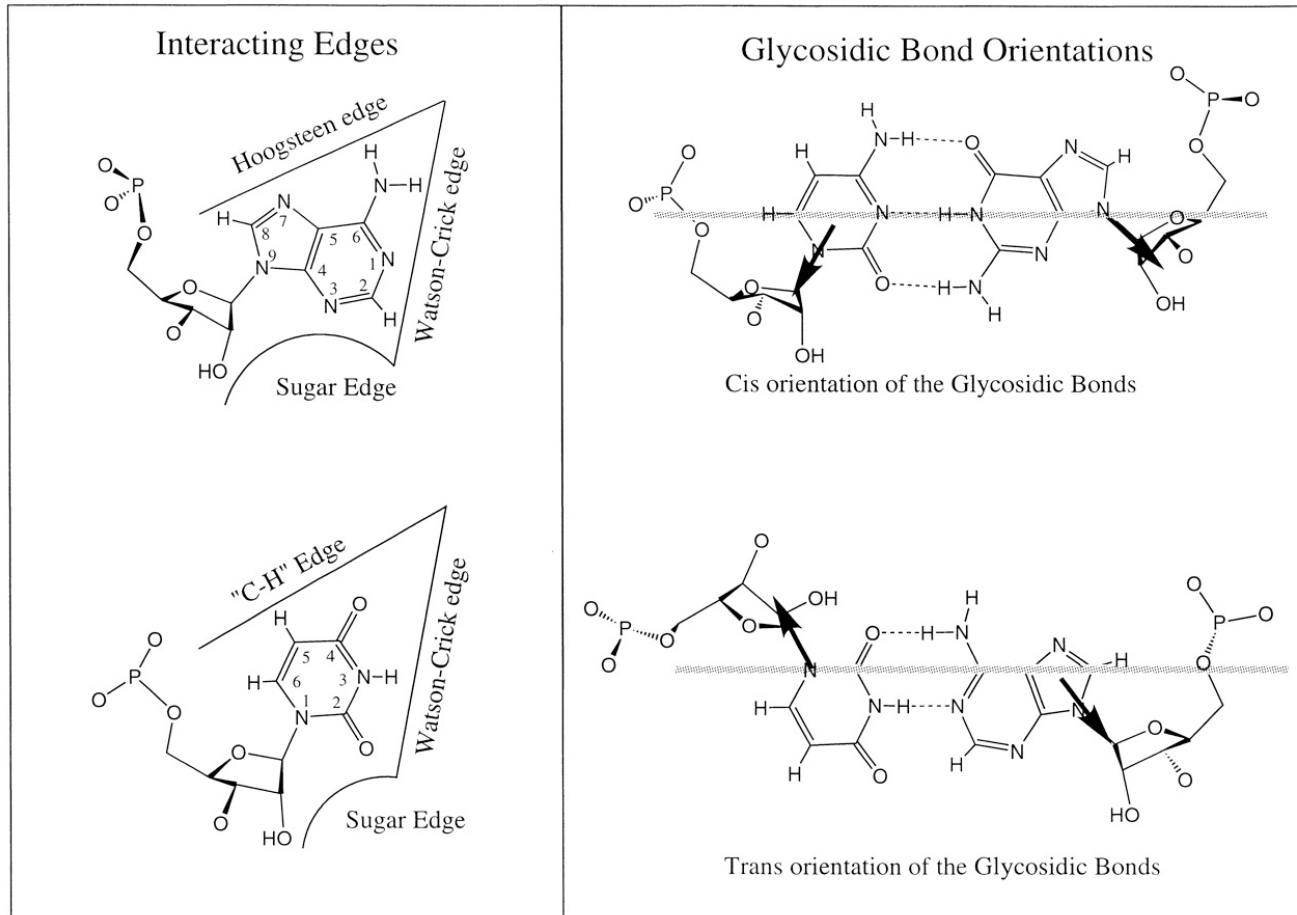
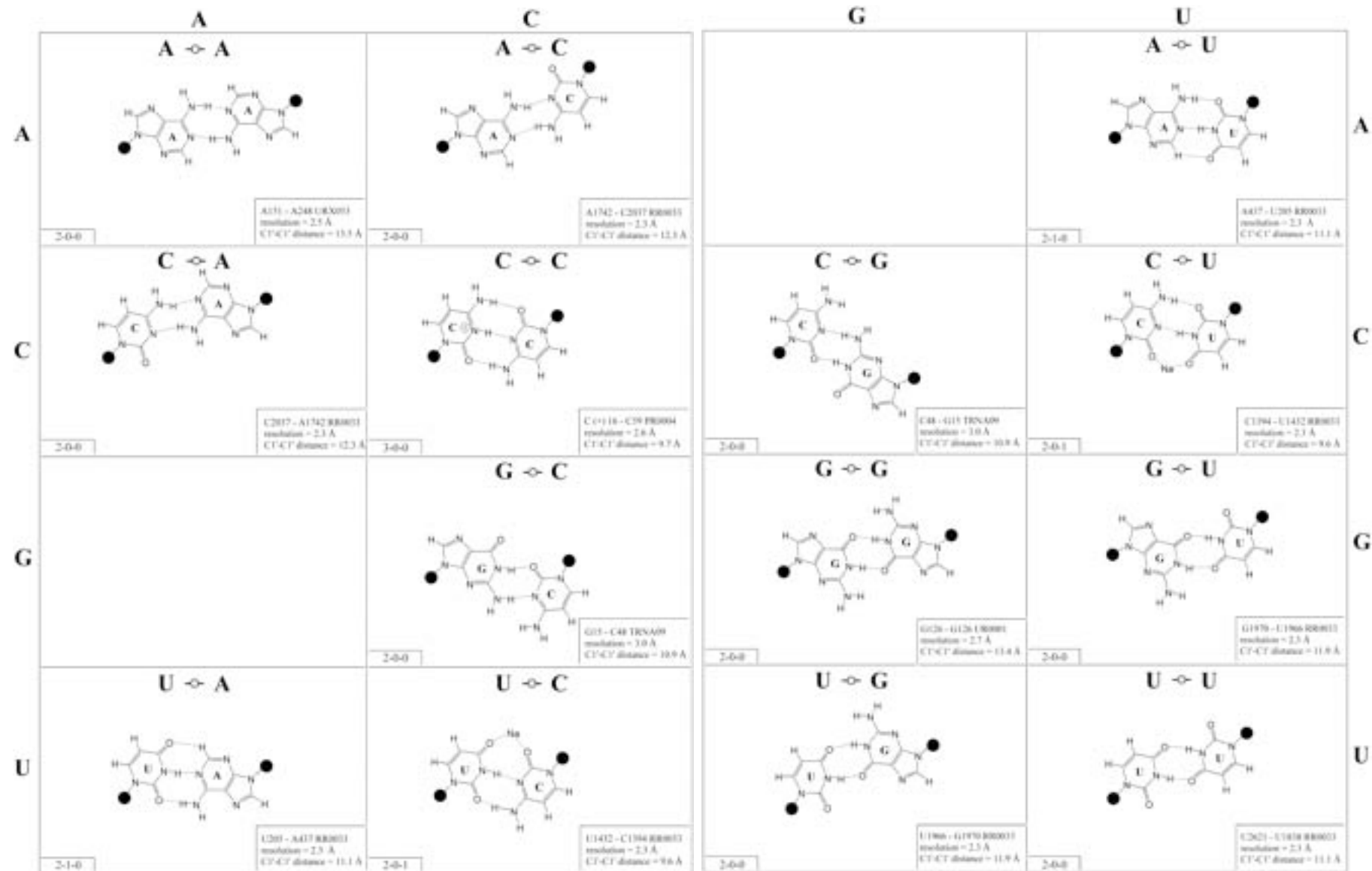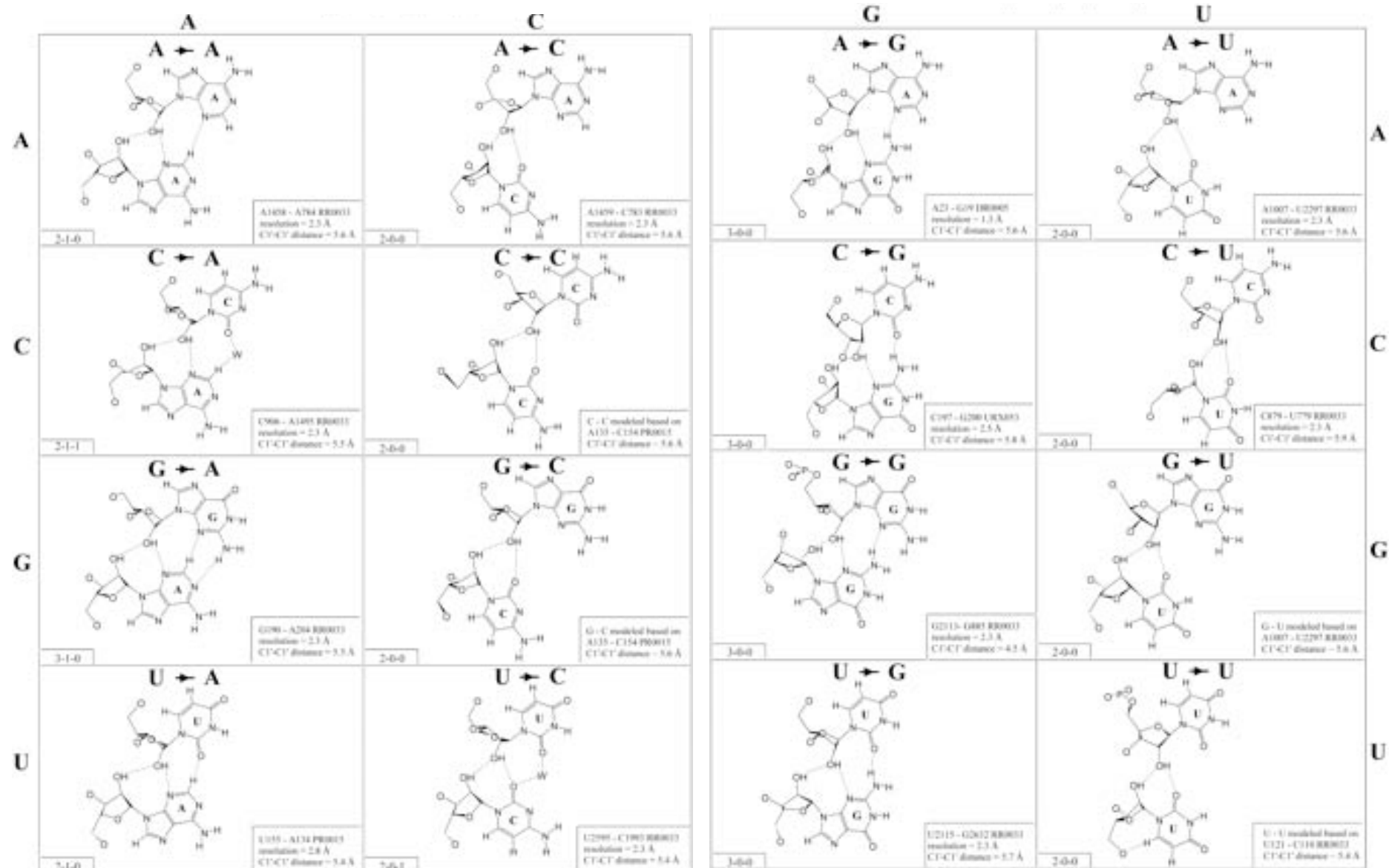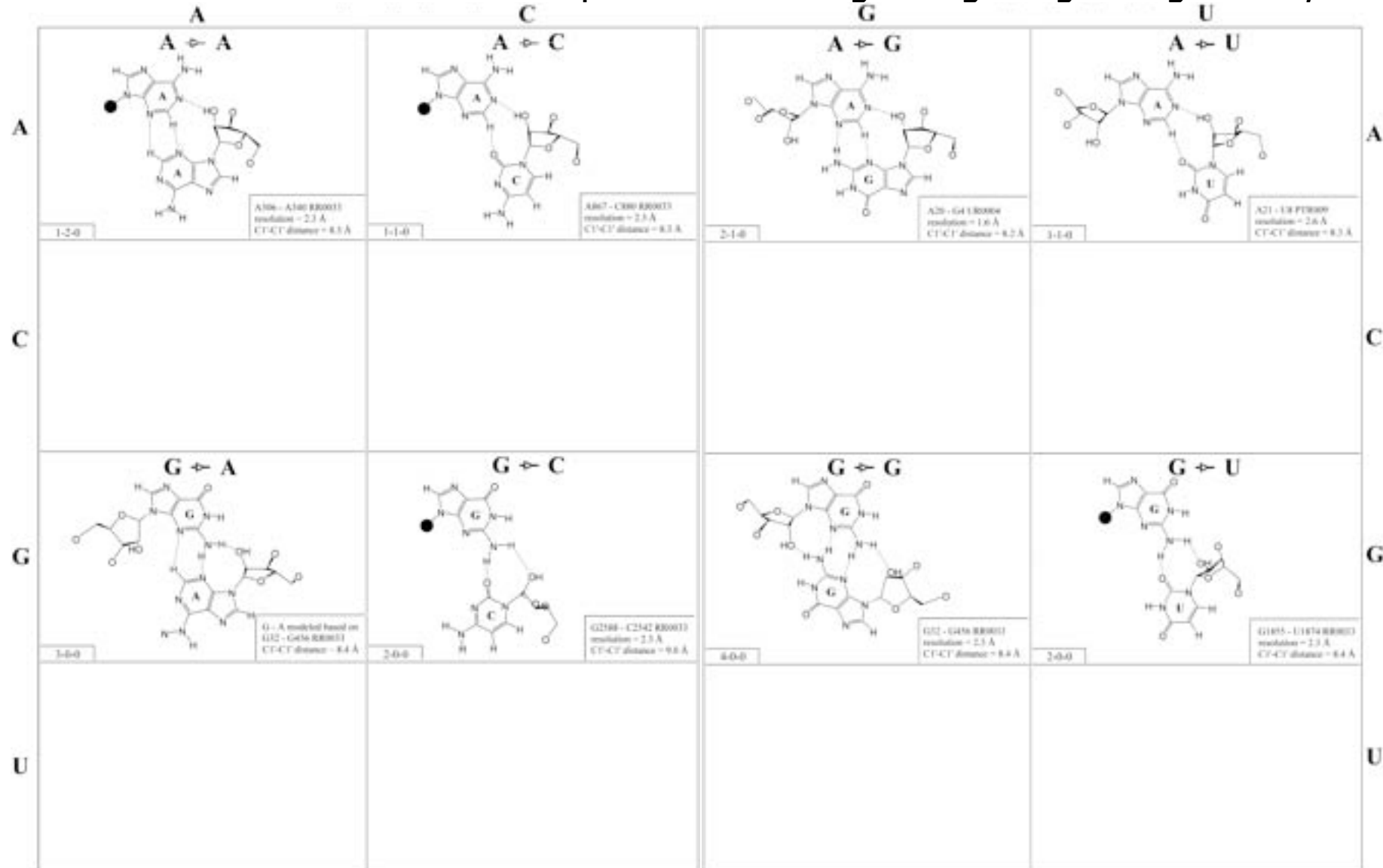cis versus trans orientation of glycosidic bonds

Leontis et al. (2002) "The non-Watson-Crick base pairs and their associated isostericity matrices." *Nucleic Acids Res.* 30, 3497-3531.

Observed base pairs in *cis* Watson–Crick/Watson–Crick family

Leontis et al. (2002) "The non-Watson-Crick base pairs and their associated isostericity matrices."
Nucleic Acids Res. 30, 3497-3531.

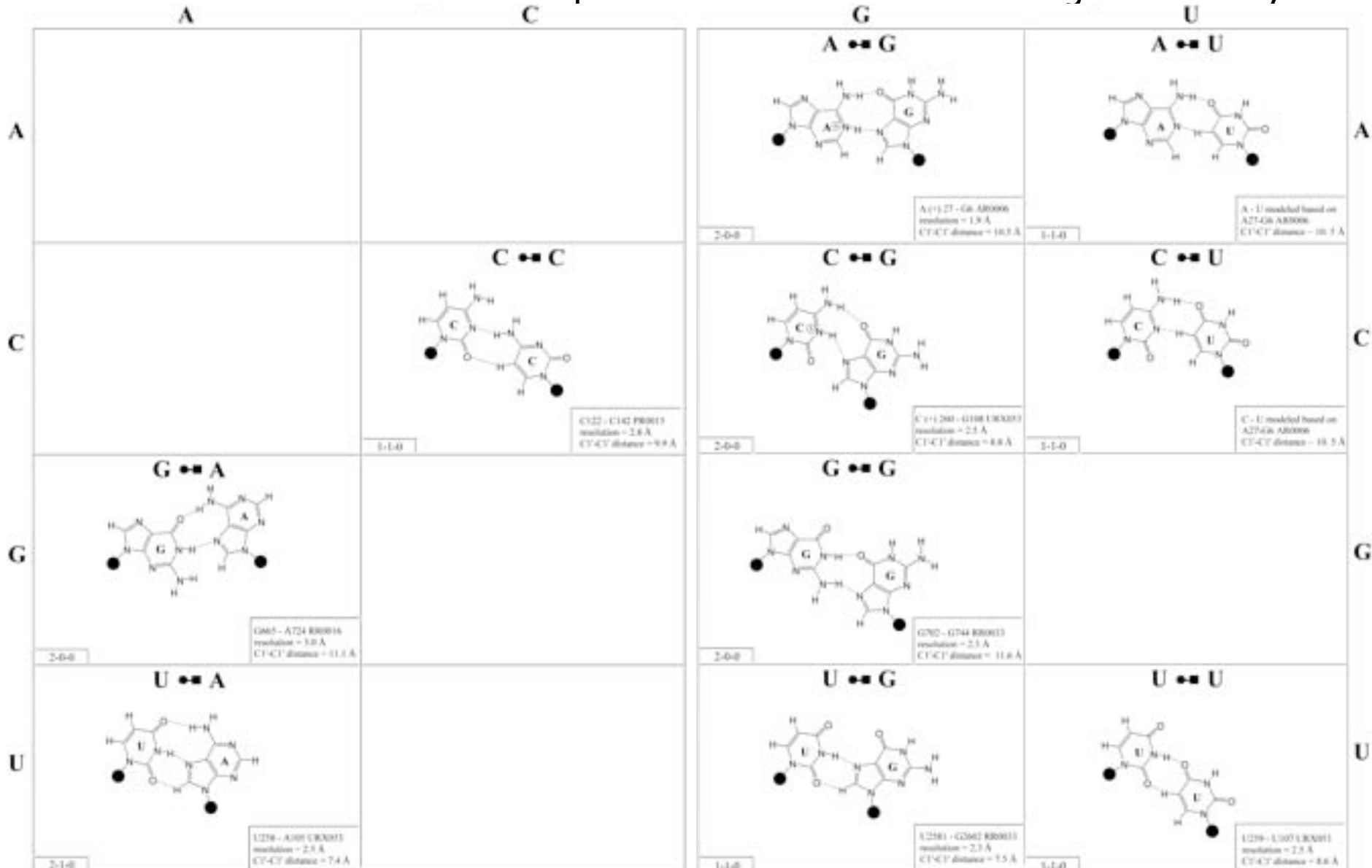# Observed base pairs in *trans* Watson–Crick/Watson–Crick family

Leontis et al. (2002) "The non-Watson-Crick base pairs and their associated isostericity matrices."
Nucleic Acids Res. 30, 3497-3531.

Observed and modeled base pairs in *cis* sugar-edge/sugar-edge family

Leontis et al. (2002) "The non-Watson-Crick base pairs and their associated isostericity matrices."
Nucleic Acids Res. 30, 3497-3531.

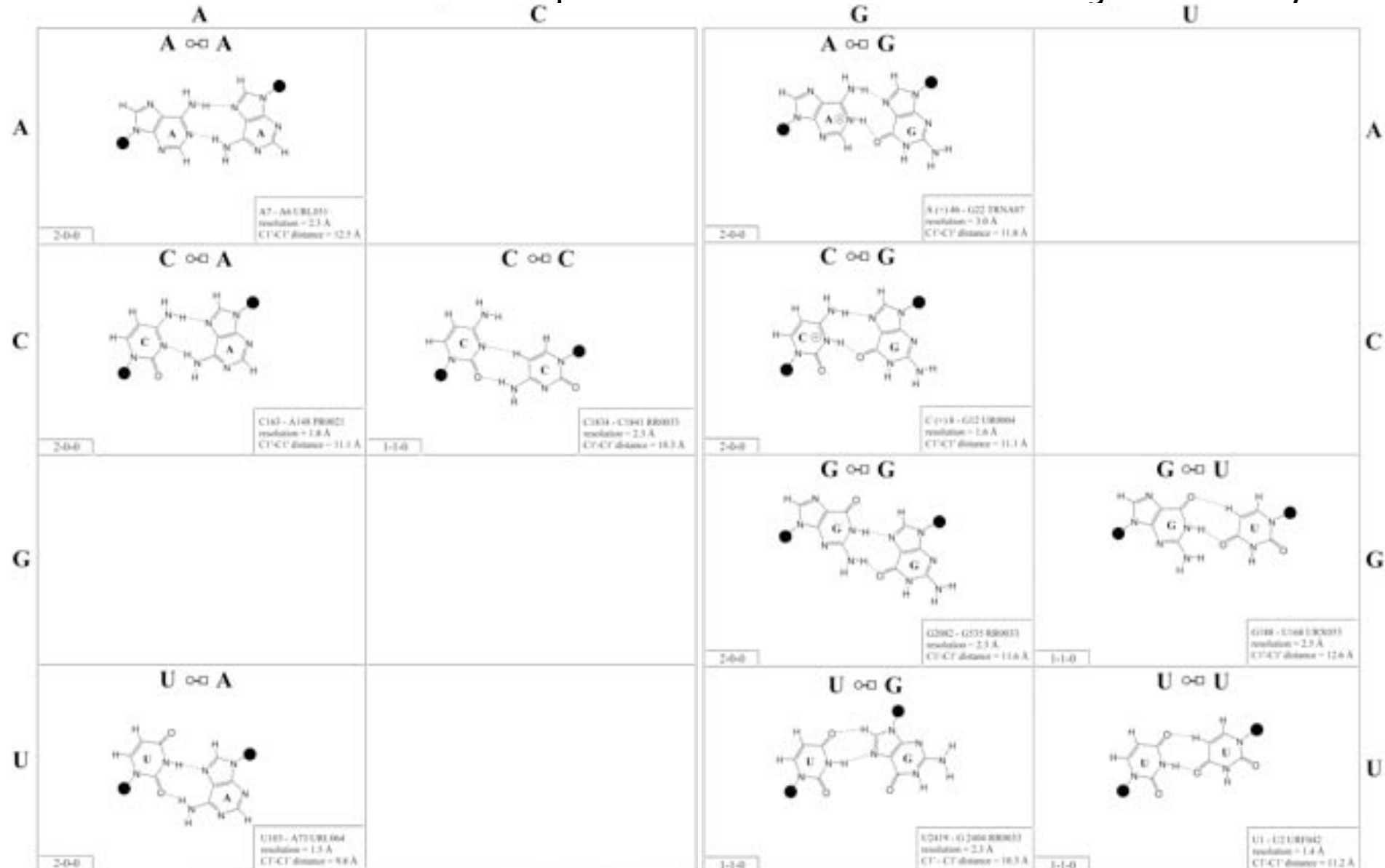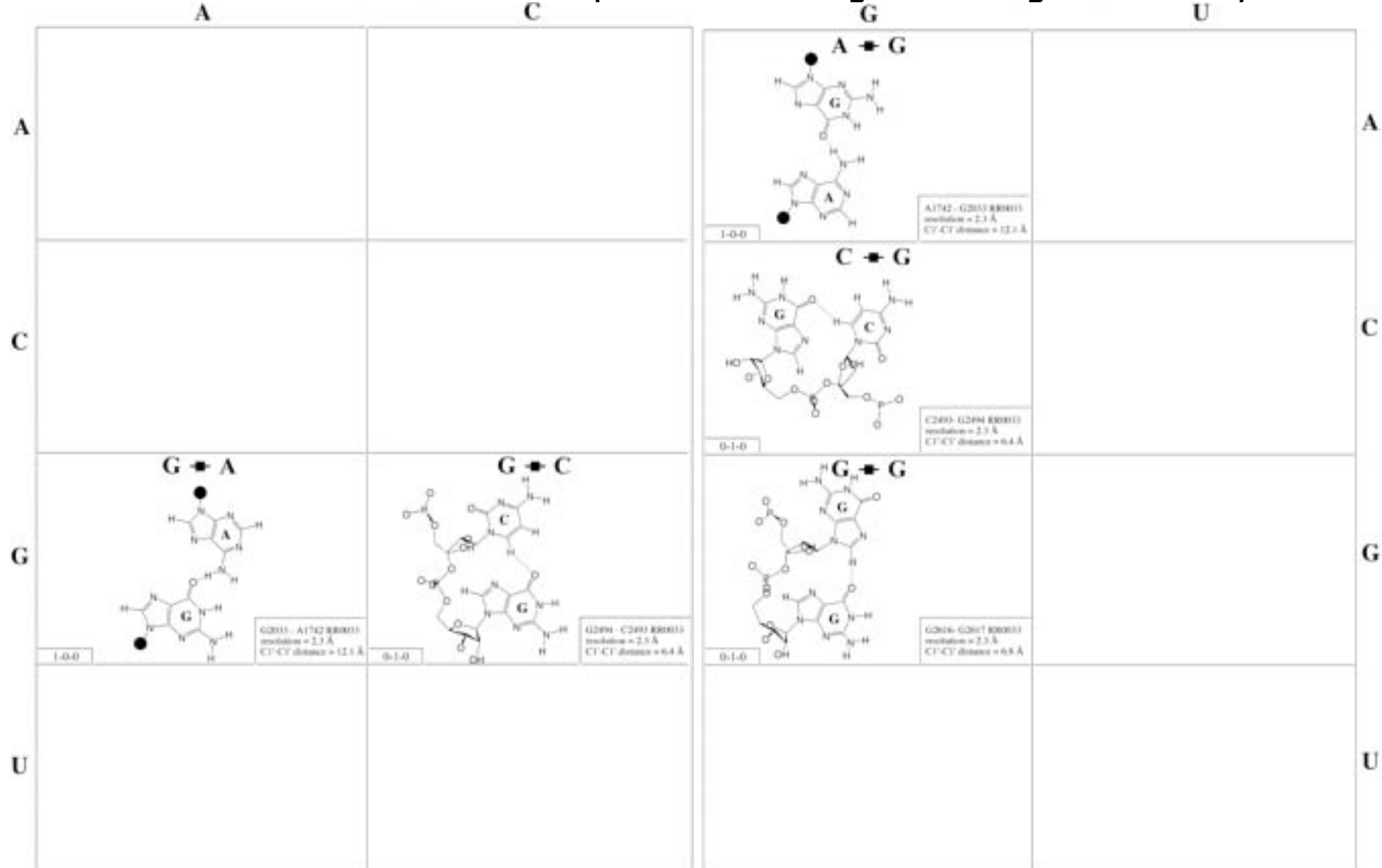# Observed and modeled base pairs in *trans* sugar-edge/sugar-edge family

Leontis et al. (2002) "The non-Watson-Crick base pairs and their associated isostericity matrices."
Nucleic Acids Res. 30, 3497-3531.

Observed and modeled base pairs in *cis* Watson–Crick/Hoogsteen family

Leontis et al. (2002) "The non-Watson-Crick base pairs and their associated isostericity matrices."
Nucleic Acids Res. 30, 3497-3531.

Observed and modeled base pairs in *trans* Watson–Crick/Hoogsteen family
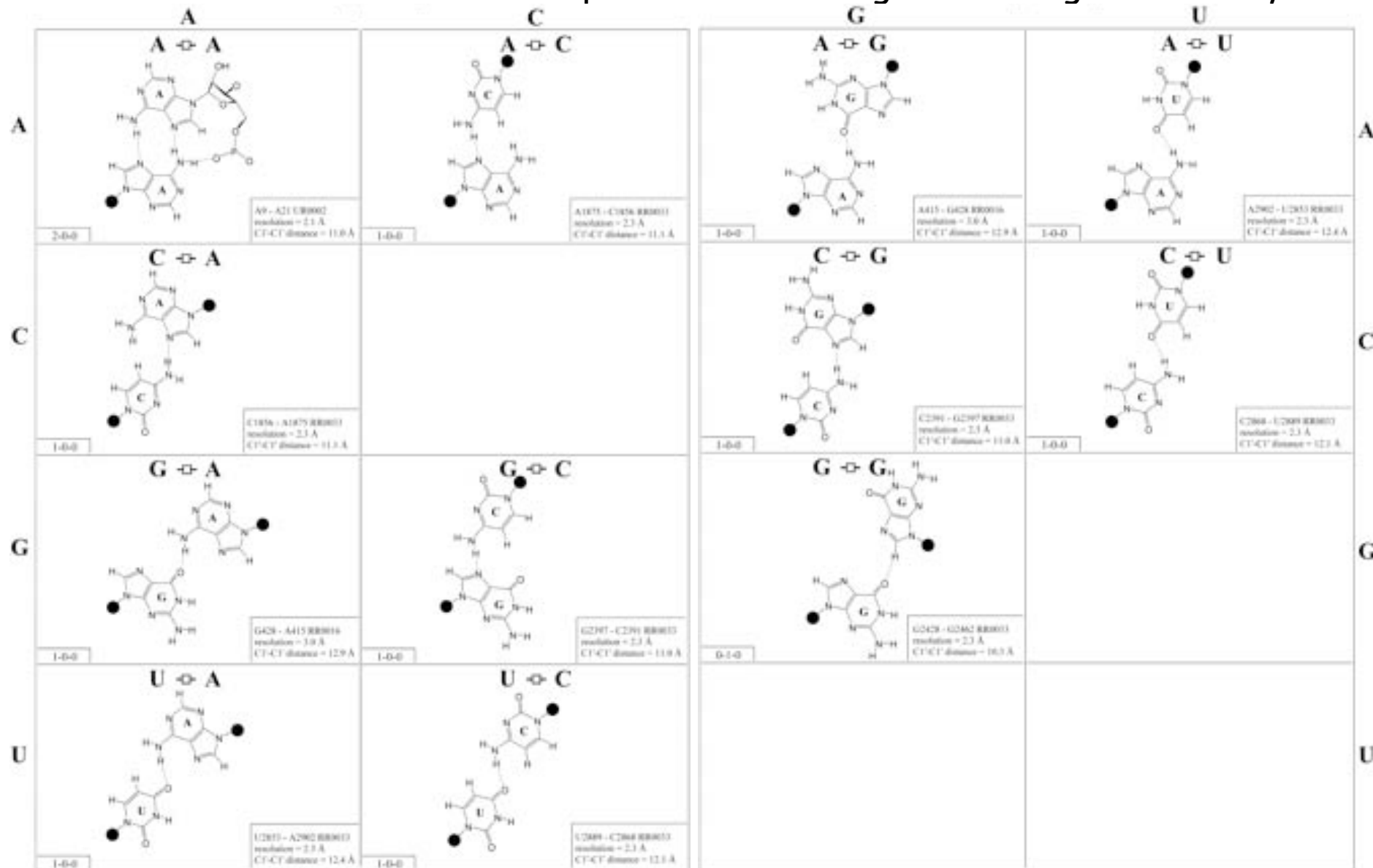

Leontis et al. (2002) "The non-Watson-Crick base pairs and their associated isostericity matrices." *Nucleic Acids Res.* 30, 3497-3531.

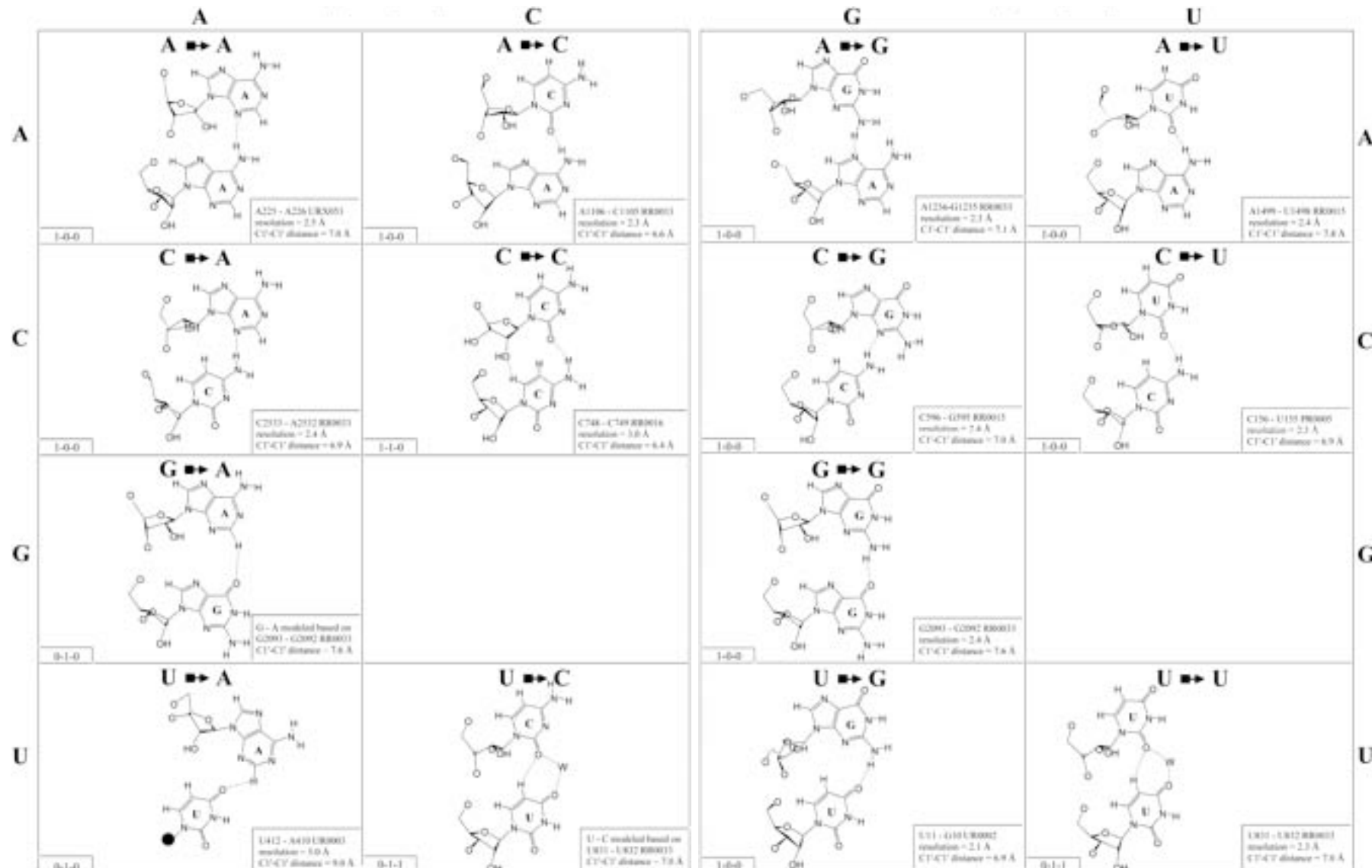# Observed and modeled base pairs in *cis* Hoogteen/Hoogsteen family

Leontis et al. (2002) "The non-Watson-Crick base pairs and their associated isostericity matrices." *Nucleic Acids Res.* 30, 3497-3531.

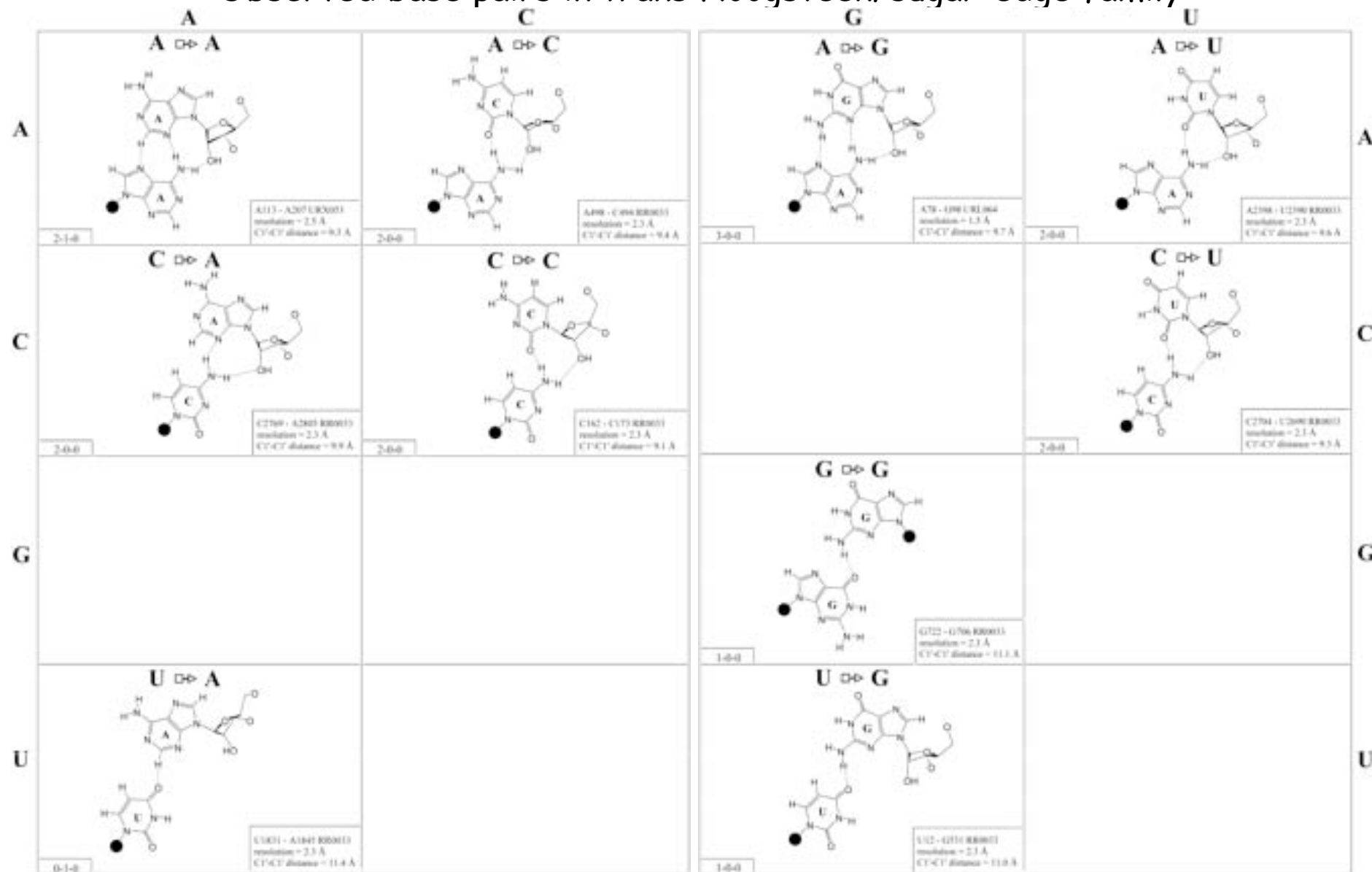# Observed and modeled base pairs in *trans* Hoogsteen/Hoogsteen family

Leontis et al. (2002) "The non-Watson-Crick base pairs and their associated isostericity matrices."
Nucleic Acids Res. 30, 3497-3531.

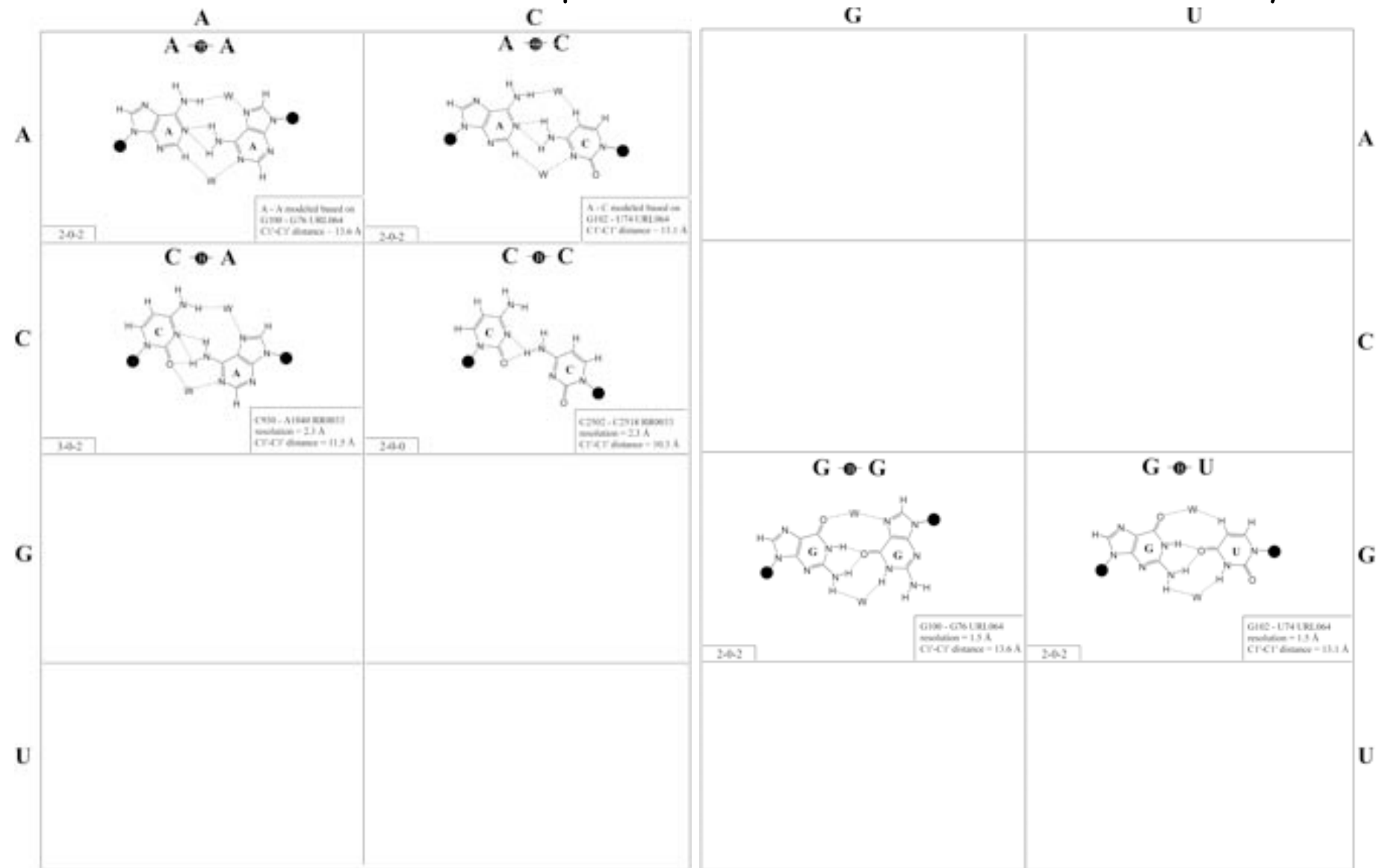# Observed and modeled base pairs in *cis* Hoogsteen/sugar-edge family

Leontis et al. (2002) "The non-Watson-Crick base pairs and their associated isostericity matrices."
Nucleic Acids Res. 30, 3497-3531.

Observed base pairs in *trans* Hoogsteen/sugar-edge family

Observed and modeled base pairs in *cis* Watson–Crick bifurcated family

Leontis et al. (2002) "The non-Watson-Crick base pairs and their associated isostericity matrices."
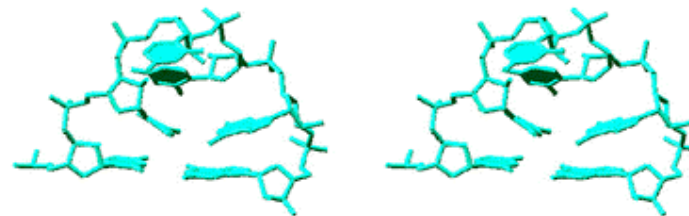*Nucleic Acids Res.* 30, 3497-3531.

Structural motifs in RNA
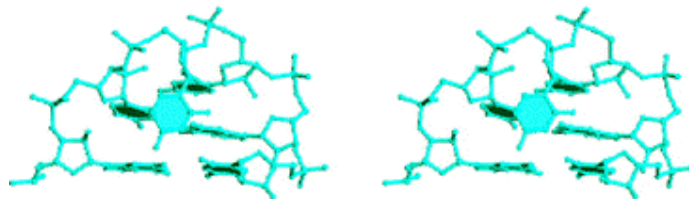
Stereoviews of three terminal-loop motifs

U-turn from anticodon
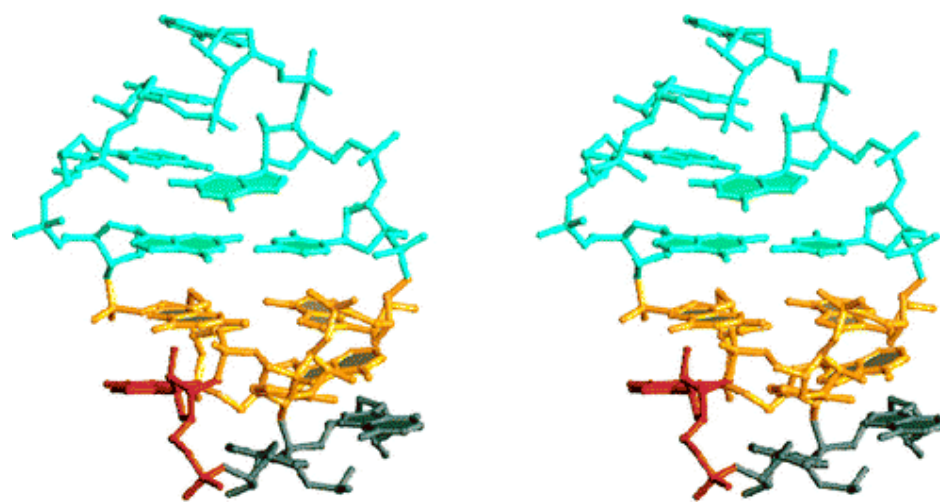loop of yeast tRNA[Phe]

UNCG tetraloop

CUYG tetraloop

A terminal loop is any sequence in which RNA folds back on itself to form a helical stem.
A terminal-loop motif is a sequence that frequently occurs in a terminal loop.

P.B. Moore. (1999) "Structural motifs in RNA." *Ann Rev. Biochem.* 68, 287-300.

Stereoview of the top of the sarcin-ricin loop - a concatenation of RNA motifs

(aqua) GNRA tetraloop of sequence GAGA, closed by a Watson-Crick G·C pair; (gold) cross-strand A stack of reversed Hoogsteen base pairs; (red) bulged G of a bulged-G motif; (gray) the symmetric A·A. Note kink in backbone at bulged G.

P.B. Moore. (1999) "Structural motifs in RNA." *Ann Rev. Biochem.* 68, 287-300.

Stereoview of a bulge-helix-bulge motif - a 7-nt internal loop that interrupts what would otherwise by a continuous A-form helix
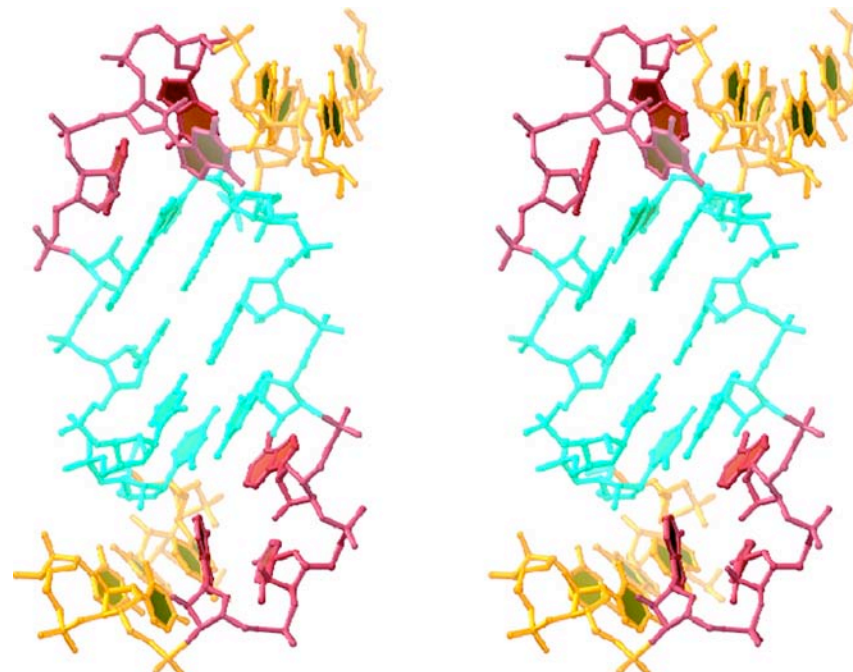
View down the approximate twofold axis from the minor groove side of the central helix. (cyan) central, 4-bp helix of the motif; (gold) base pairs of the larger helix, which the motif interrupts; (red) two 3-nt bulges (sites of splicing in Archaea)
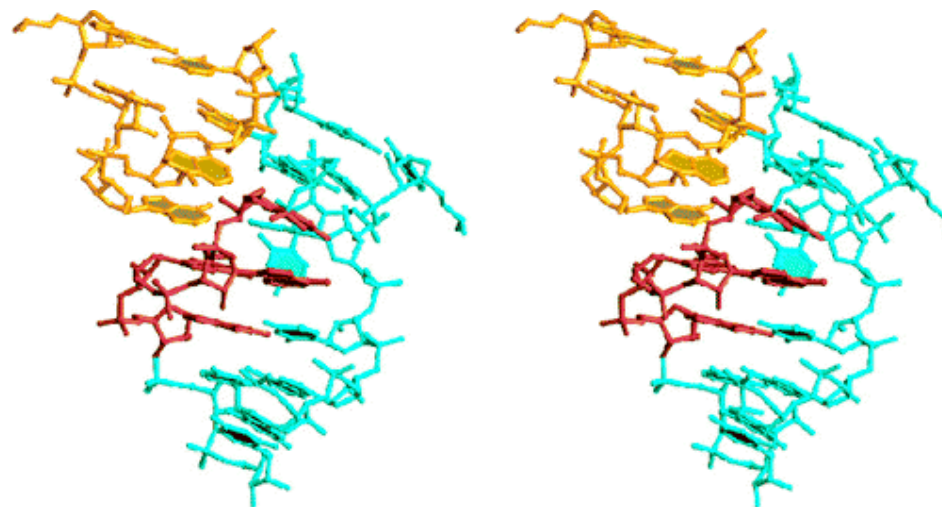
P.B. Moore. (1999) "Structural motifs in RNA." *Ann Rev. Biochem.* 68, 287-300.

Stereoview of a ribose zipper (tertiary) motif - two strands of RNA held in place by a network of H bonds in which the 2´ -OH groups of two consecutive riboses on both strands are the principal players

View from the backbone side, looking approximately down the pseudo-twofold axis of motif

P.B. Moore. (1999) "Structural motifs in RNA." *Ann Rev. Biochem.* 68, 287-300.

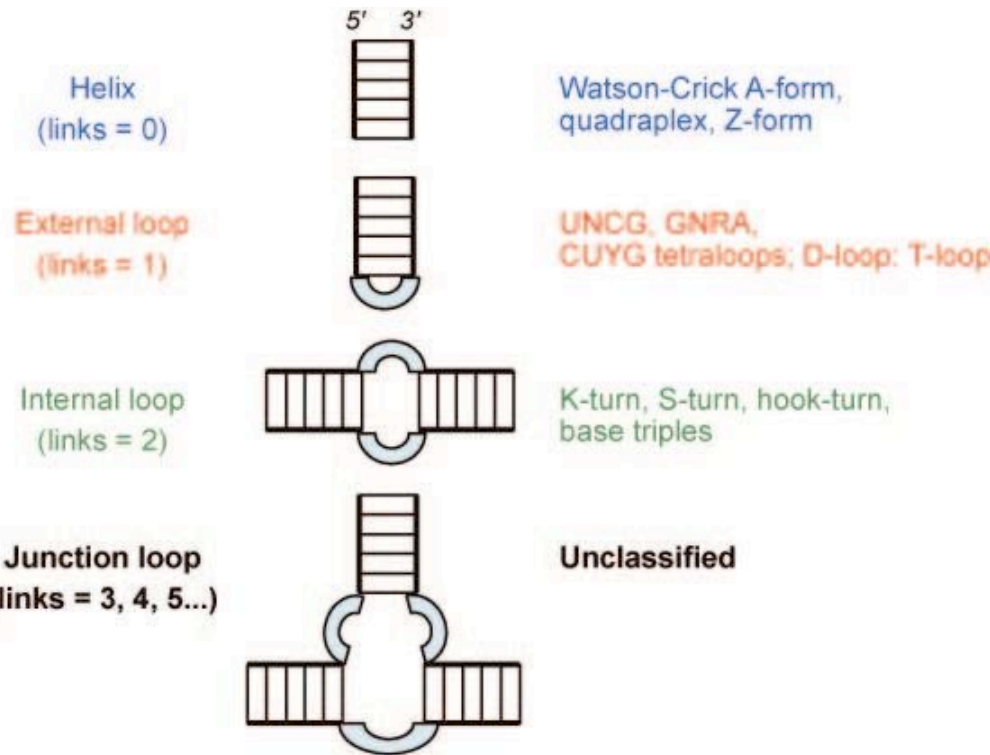# Stereoview of a tetraloop docked with a tetraloop receptor
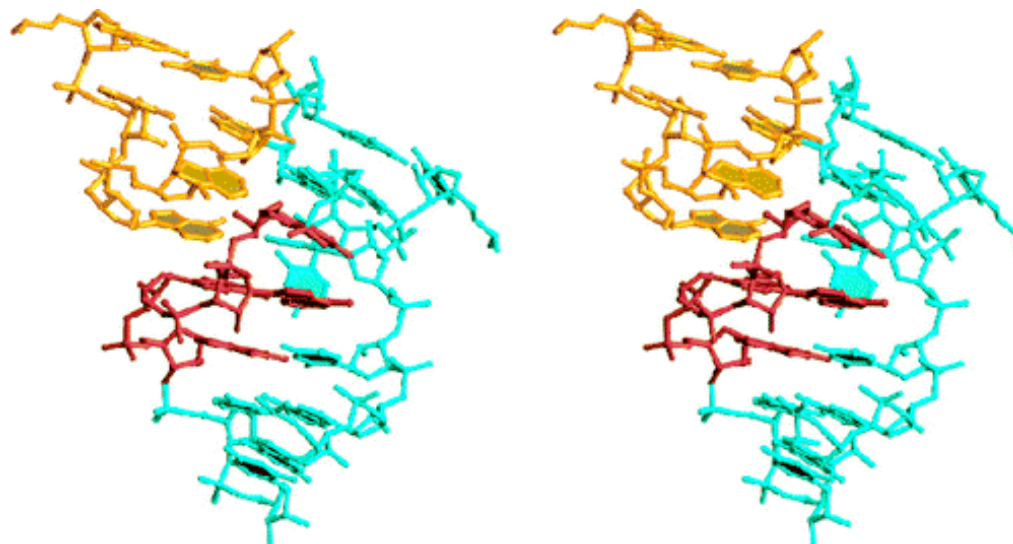
(gold) GNRA tetraloop; (red) four bases, at the center of the tetraloop receptor, which are the heart of the A-platform. Note the stacking of the middle two adenines on the bases of the supporting helix. (cyan) remainder of the receptor

P.B. Moore. (1999) "Structural motifs in RNA." *Ann Rev. Biochem.* 68, 287-300.

Structural principles from large RNAs

Schematic illustrating types of secondary structure found in RNA

	5' 3'	
Helix (links = 0)		Watson-Crick A-form, quadraplex, Z-form
External loop (links = 1)		UNCG, GNRA, CUYG tetraloops; D-loop; T-loop
Internal loop (links = 2)		K-turn, S-turn, hook-turn, base triples
Junction loop (links = 3, 4, 5...)		Unclassified

Ladders - double helices. Blue semicircles - single-stranded linkers (connecting helices). Examples of secondary structural types are listed on the right.

S.R. Holbrook. (2008) "Structural principles from large RNAs." *Ann Rev. Biophys.* 37, 445-464.

Continuous interhelical stack in P4-P6 domain of group I intron (PDB_ID 1gid)
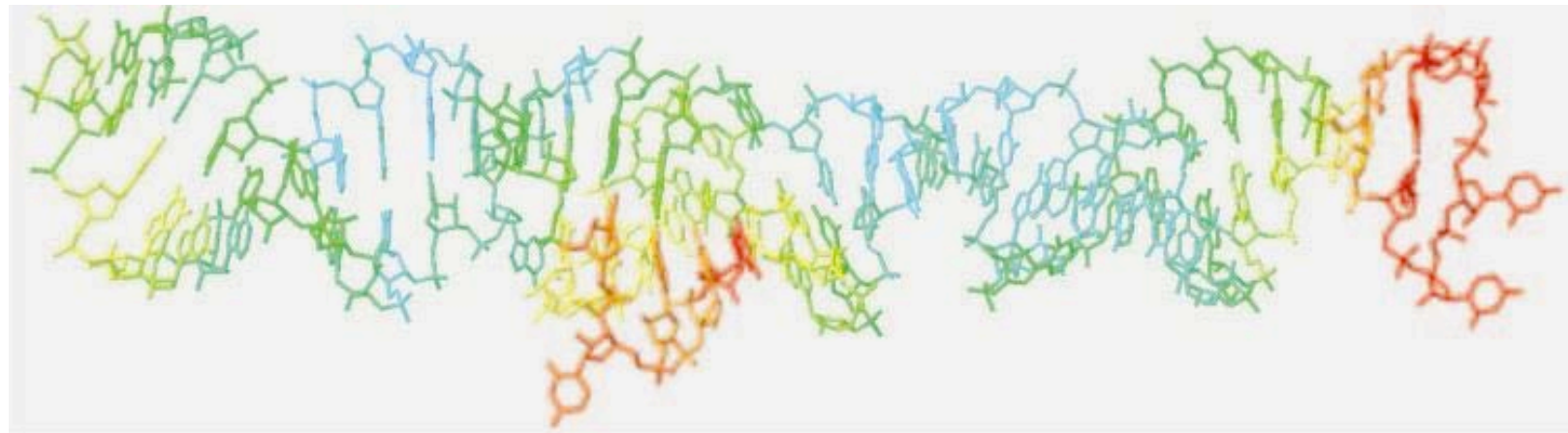

Stack includes four double-helical regions, three internal loops, and a hairpin loop, spanning 78 residues. Residues color coded by B-factor (mobility); the red/orange in hairpin loop (end of stack) and at 5′ - and 3′ -ends (middle of stack) are most mobile. Stacked residues generally less mobile.
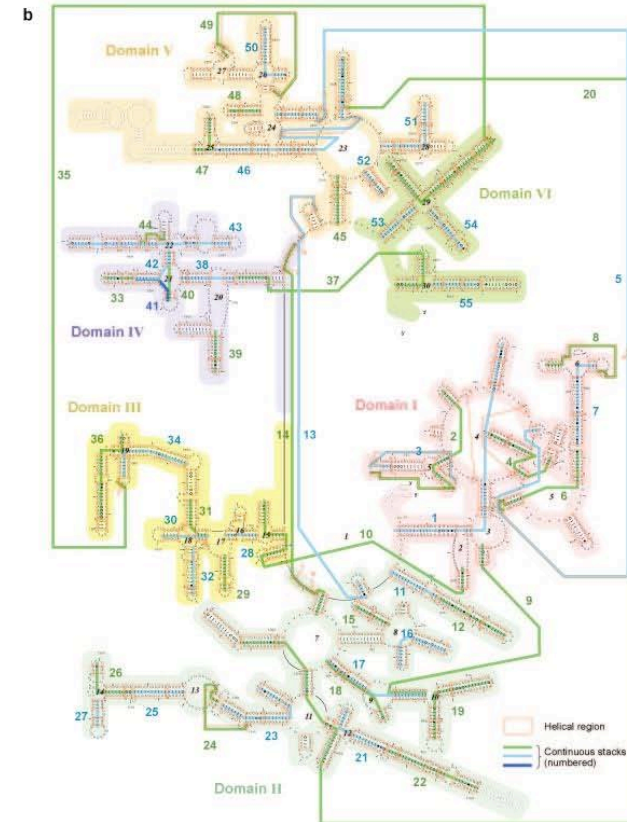
S.R. Holbrook. (2008) "Structural principles from large RNAs." *Ann Rev. Biophys.* 37, 445-464.

COIN stacks in ribosomal RNAs

COntinuous INterhelical base stacking; extended base stacks formed from multiple double helices
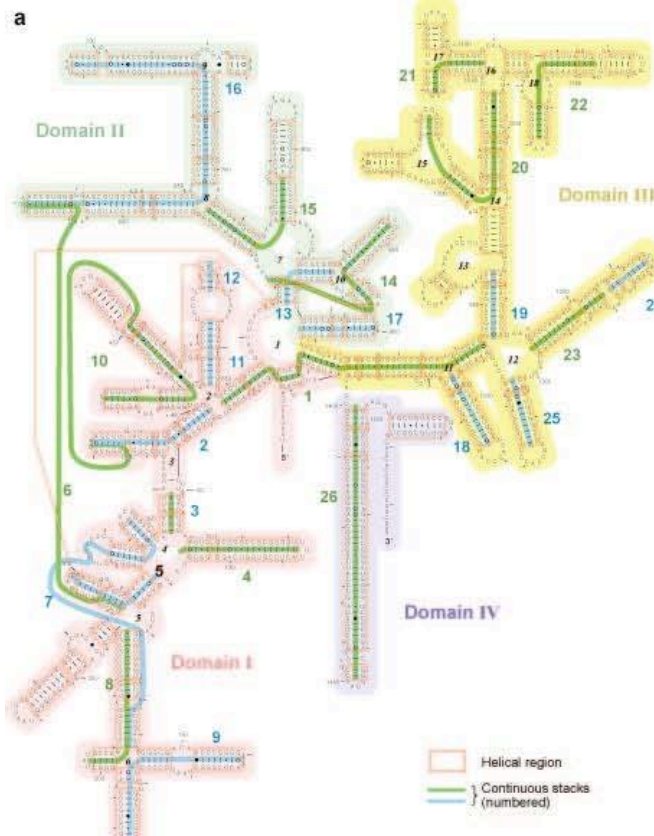
Thermus thermophilus 16S rRNA

Haloarcula marismortui 23S rRNA

Domains - shaded and labeled with Roman numerals. Junction loop numbers - italics. Helical regions enclosed by red rectangles and continuous stacks - green or blue highlights and numbered

S.R. Holbrook. (2008) "Structural principles from large RNAs." *Ann Rev. Biophys.* 37, 445-464.
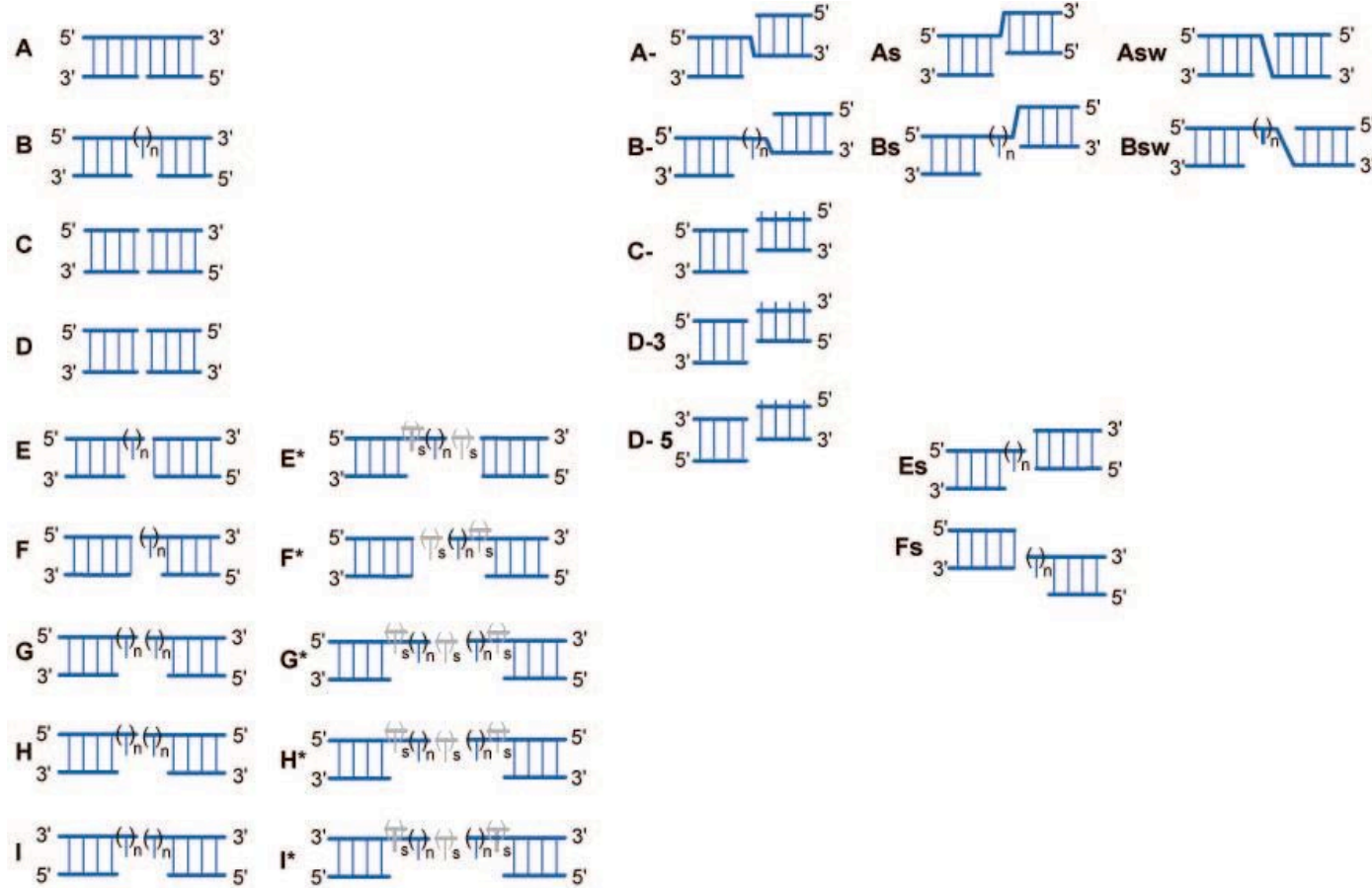
'Kissing' hairpin loops show continuous base stacking in ribosomal RNA.

Blue and violet correspond to different external (hairpin) loops

S.R. Holbrook. (2008) "Structural principles from large RNAs." *Ann Rev. Biophys.* 37, 445-464.
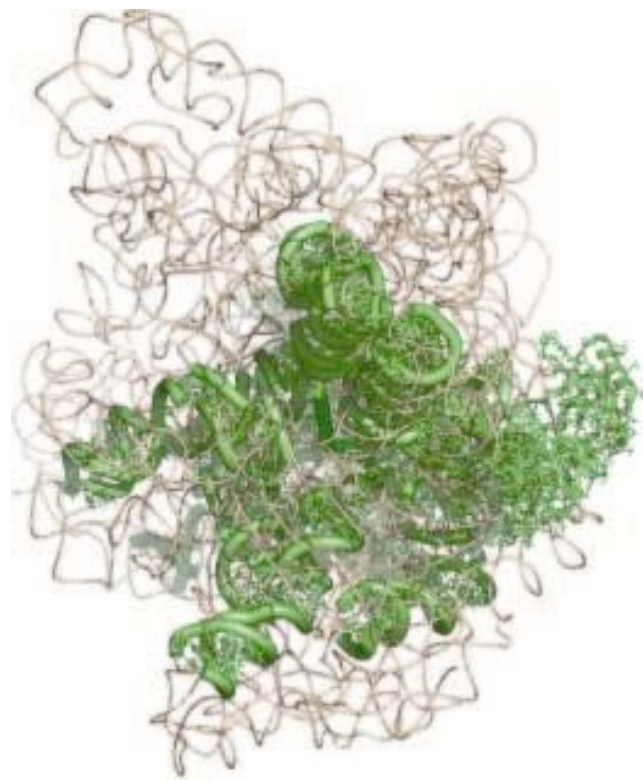
10 major classes of bridging between continuously stacked RNA double helices

Interhelical bridge classifications shown as ladders with 5´- and 3´-ends labeled.

S.R. Holbrook. (2008) "Structural principles from large RNAs." *Ann Rev. Biophys.* 37, 445-464.

# Polypeptide exit tunnel of the 50S ribosomal subunit formed by COIN stacking.

Thin green ribbons are protein and thick green tubes correspond to COIN stacks that form the tunnel. Brown strands trace the backbone of the remainder of the rRNA.

S.R. Holbrook. (2008) "Structural principles from large RNAs." *Ann Rev. Biophys.* 37, 445-464.

Domains in *Thermus thermophilus* 16S rRNA.
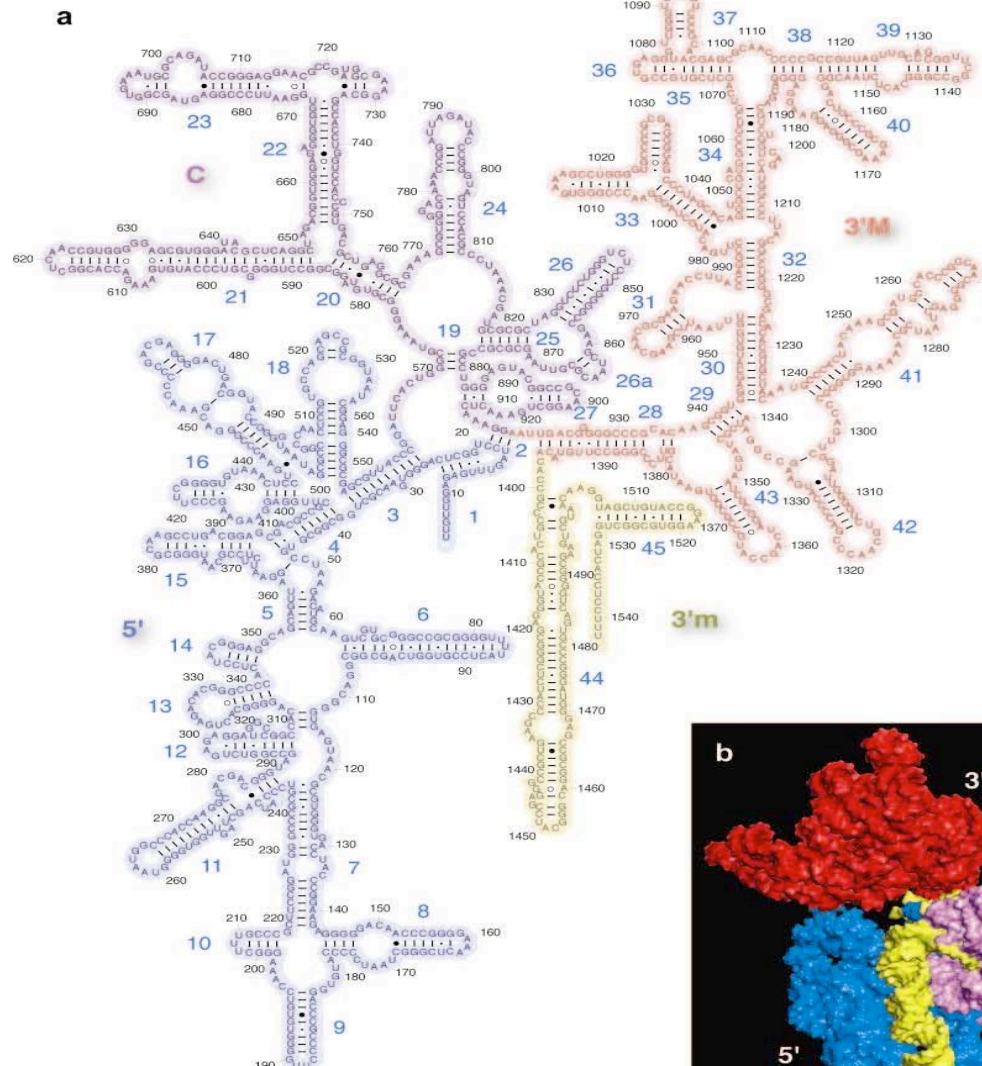
Domains 5′, c, 3′M, 3′m correspond respectively to domains I, II, III, IV.
(a) Domains defined by secondary structure.
(b) Secondary structure domains shown in tertiary structure. Color coding the same in both domains
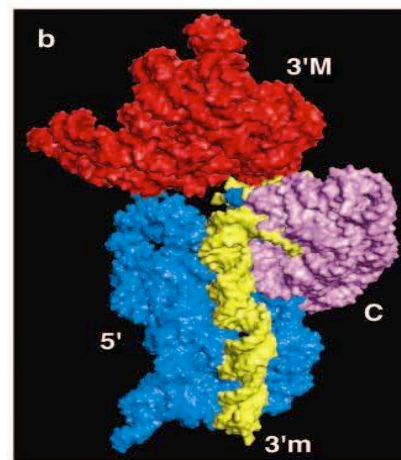
S.R. Holbrook. (2008) "Structural principles from large RNAs." *Ann Rev. Biophys.* 37, 445-464.

General architecture of large RNAs.
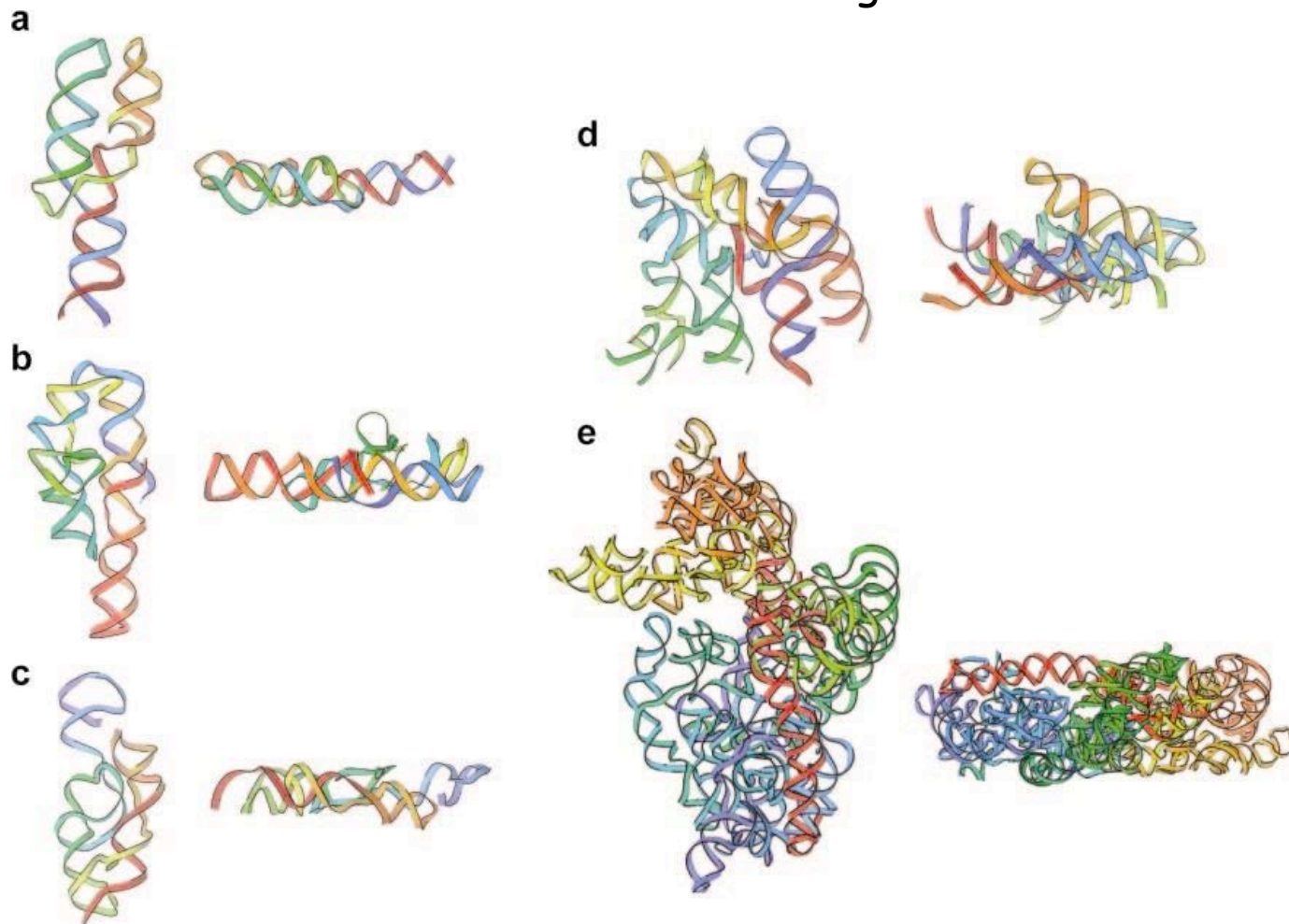
Ribbon representation color-coded such that the color varies from blue to red as the chain progresses. Two views of (a) S-domain complex of human signal recognition particle (PDBID 1mfq). (b) P4-P6 domain of group I intron (1gid). (c) GlmS ribozyme (2nz4). (d) RNAse P RNA (2a64). (e) 16S rRNA (1j5e).

S.R. Holbrook. (2008) "Structural principles from large RNAs." *Ann Rev. Biophys.* 37, 445-464.

Electronic Resources

Molecular images of RNA
"Ribosome structure and tRNA binding site (3-D structure)" – Joachim Frank:
http://www.dnatube.com/video/59/Ribosome-structure-and-trna-binding-site--3-D-structure-

"Visualization of tRNA Movements on 70S Ribosome" – Joachim Frank:
http://www.dnatube.com/gvideos.php?viewkey=aa6e02c990b0a82652dc&urlkey=trna&gid=34

"tRNA-Ribosome Molecular Dynamics Simulation" – Sanbonmotsu et al.
http://www.pnas.org/content/102/44/15854/suppl/DC1#M1

tRNA structure 2D
http://www.dnatube.com/video/719/tRNA-structure-2D

Useful introductory materials:

PBS ScienceNOW (July 26, 2005) "How is RNAi discovered" – Robert Krulwich:
http://www.pbs.org/wgbh/nova/sciencenow/3210/02.html

HHMI 1995 Holiday Lecture "The double life of RNA" – Tom Cech
http://www.hhmi.org/biointeractive/rna/lectures.html

Henry Stewart Talks – "From DNA to Proteins: The Multiple Levels of Regulation"
 http://www.hstalks.com/main/browse_talks.php?father_id=22&c=252
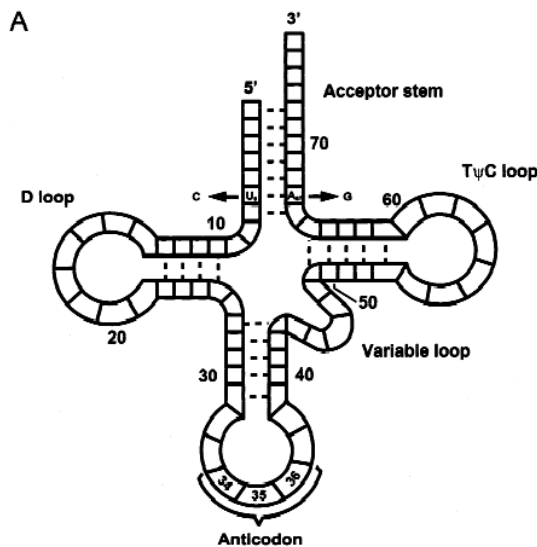
Lectures by leading researchers:
NIH videocasts:
http://videocast.nih.gov/Search.asp

IMA Lectures 2007 Workshop on RNA in Biology, Bioengineering, and Nanotechnology:
http://www.ima.umn.edu/2007-2008/W10.29-11.2.07/abstracts.html

Deconstructing and reconstructing transfer RNA – PDB_ID 1ehz
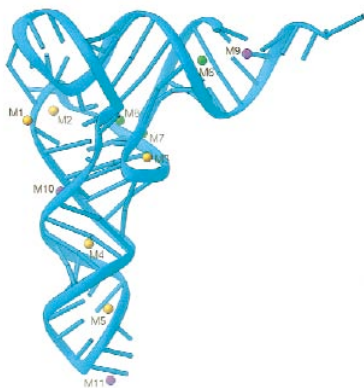

Holliday junction 2°-structure of yeast tRNA^{Phe} (Image from Shi & Moore (2000))

Acceptor   D   D   Acodon   Acodon   TψC   TψC Acceptor

GCGGAUUUAgCUCAGuuGGGAGAGCgCCAGAcUgAAgAPcUGGAGgUCcUGUGuPCGaUCCACAGAAUUCGCACCA
1234567890123456789012345678901234567890123456789012345678901234567890123456

1. Identification of continuosuly stacked helical regions

Tertiary structure of yeast tRNA^Phe (Shi & Moore (2000); PDB_ID 1ehz)

```
Continuously stacked structural segments
GCGGAUUUUAgCUCAGuuGGGAGAGCgCCAGAcUgAAgAPcUGGAGgUCcUGUGuPCGaUCCACAGAAUUCGCACCA h1 h2 h3
1234567890123456789012345678901234567890123456789012345678901234567890123456

Composite of 2° and 3° features
GCGGAUUUAgCUCAGuuGGGAGAGCgCCAGAcUgAAgAPcUGGAGgUCcUGUGuPCGaUCCACAGAAUUCGCACCA
1234567890123456789012345678901234567890123456789012345678901234567890123456


>>>>>>>        <                      >>>>>>>  <  <<<<<<<<<<<<  h1 accptrTψC
     < >>>>>>>     <<<<<<<<<<<< >  >>>>>>>   <           <      h2 AcodonD
            +                                   +             h3 DTψCloops
```

2. Non-canonical base-pair notation and H-bonding

(a) noncanonical bases in h1
```
GCGGAUUUAgCUCAGuuGGGAGAGCgCCAGAcUgAAgAPcUGGAGgUCcUGUGuPCGaUCCACAGAAUUCGCACCA h1
1234567890123456789012345678901234567890123456789012345678901234567890123456
>>>>>>>>           <                              >>>>>>>  <   <<<<<<<<<<<   h1 accptrTψC
```
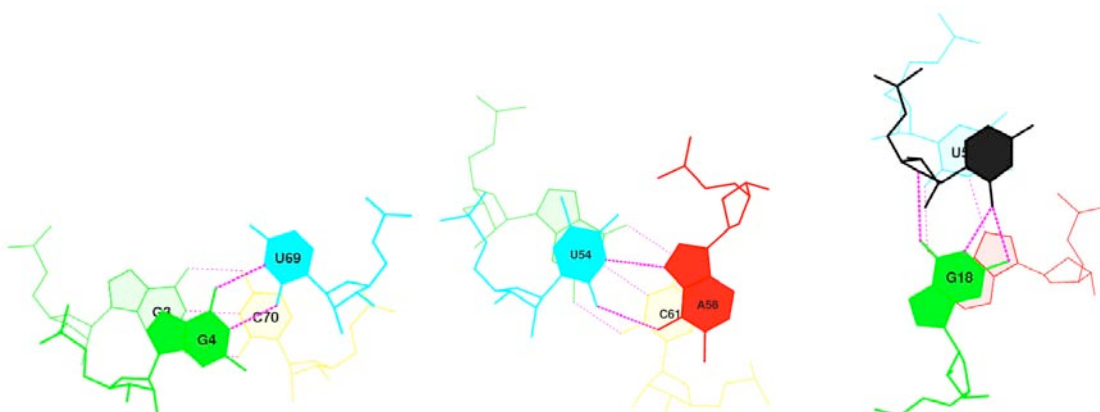

Illustration of three steps from the h1 continutous stack with noncanonical base pairs:
(left) G3G4·U69C70;(center) G53u54·A58C61; (right) u54P55·G18a58

(b) noncanonical bases in h2
```
GCGGAUUUAgCUCAGuuGGGAGAGCgCCAGAcUgAAgAPcUGGAGgUCcUGUGuPCGaUCCACAGAAUUCGCACCA h2
1234567890123456789012345678901234567890123456789012345678901234567890123456
  <  >>>>>>   <<<<<<<<<<<<    >>>>>>>        <            h2 AcodonD
```
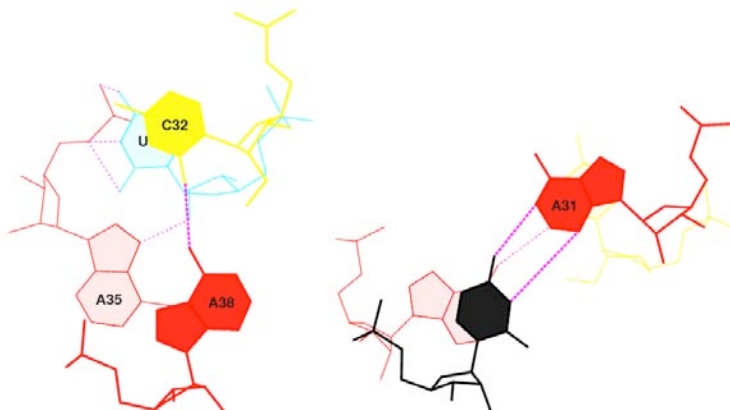

Illustration of two steps from the h2 continutous stack with noncanonical base pairs:
(left) A35A38·c32U33;(center) A38P39·A31c32

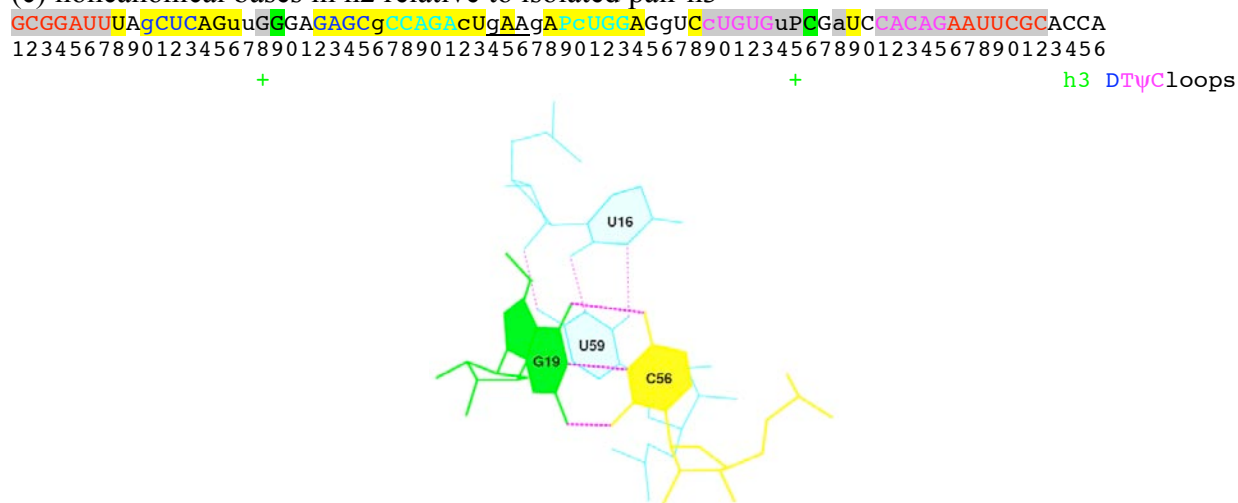(c) noncanonical bases in h2 relative to isolated pair h3

GCGGAUUUAgCUCAGuuGGGAGAGCgCCAGAcUgAAgAPcUGGAGgUCcUGUGuPCGaUCCACAGAAUUCGCACCA
12345678901234567890123456789012345678901234567890123456789012345678901234 56

　　　　　　　　+　　　　　　　　　　　　　　　　　　　　　　+　　　　　　　　　h3 DTψCloops

Illustration isolated G19·C56 pair with respect to the noncanonical U59·U16 pair in h2.

3. Angles betweem base-pair normals distinguish continuous helical stackes in tRNA[Phe]

Angle , in degrees, between consecutive bps
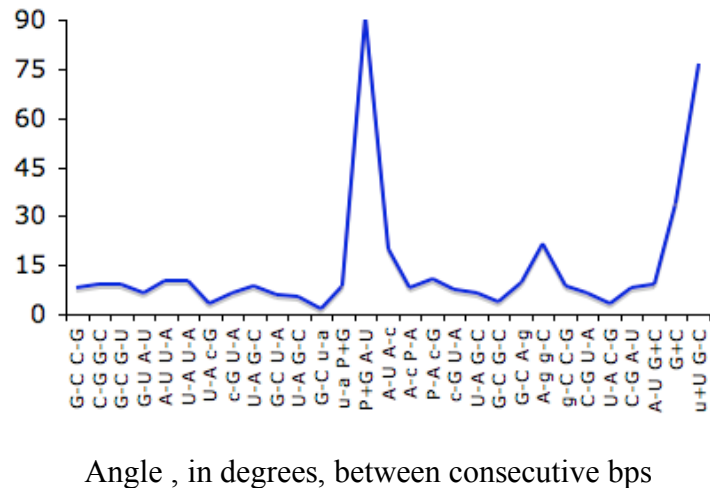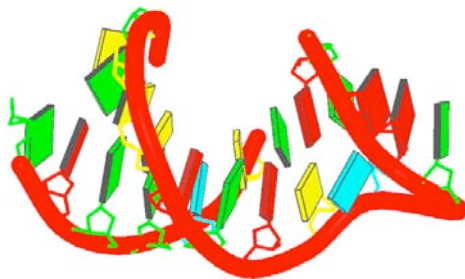
4. RNA chain reconstruction

Image of anticodon loop reconstructed from text-only file of the six step parameters relating bases 25-45 in 1ehz

Image of single-stranded structure reconstructed from text-only file of repeating base-step parameters describing adjacent nucleotides in the canonical A RNA.

Image of single-stranded structure reconstructed from text-only file of repeating base-step parameters of canonical A RNA with a central guanine arranged as in the sharp turn in the yeast tRNA^{Phe} anticodon loop.

Files for chain reconstruction:

Bases comprising two turns of A-RNA

```
22 # bases
   0 # ***local step parameters***
#    Shift   Slide   Rise   Tilt    Roll   Twist
A    0.00    0.00    0.00   0.00    0.00    0.00
A    0.02   -1.48    3.30  -0.00    8.64   31.57
A    0.02   -1.48    3.30   0.00    8.64   31.57
A    0.02   -1.48    3.30   0.00    8.63   31.56
A    0.02   -1.48    3.30   0.00    8.64   31.58
A    0.02   -1.48    3.30  -0.00    8.64   31.57
A    0.02   -1.48    3.30   0.00    8.64   31.57
A    0.02   -1.48    3.30  -0.00    8.64   31.57
A    0.02   -1.48    3.30   0.00    8.63   31.57
A    0.02   -1.48    3.30  -0.00    8.64   31.57
A    0.02   -1.48    3.30  -0.00    8.64   31.57
A    0.02   -1.48    3.30  -0.00    8.64   31.57
A    0.02   -1.48    3.30   0.00    8.64   31.57
A    0.02   -1.48    3.30  -0.00    8.63   31.56
A    0.02   -1.48    3.30   0.00    8.64   31.57
A    0.02   -1.48    3.30  -0.00    8.63   31.58
A    0.02   -1.48    3.30   0.00    8.64   31.56
A    0.02   -1.48    3.30  -0.00    8.64   31.57
A    0.02   -1.48    3.30  -0.00    8.63   31.56
A    0.02   -1.48    3.30   0.00    8.64   31.58
A    0.02   -1.48    3.30  -0.00    8.64   31.57
A    0.02   -1.48    3.30  -0.00    8.63   31.57
```

Bases comprising two turns of A-RNA plus an inserted G with parameters describing the sharp turn in the anticodon loop of yeast tRNA[Phe].

```
23 # bases
   0 # ***local step parameters***
#    Shift   Slide   Rise   Tilt     Roll    Twist
A    0.00    0.00    0.00   0.00     0.00     0.00
A    0.02   -1.48    3.30  -0.00     8.64    31.57
A    0.02   -1.48    3.30   0.00     8.64    31.57
A    0.02   -1.48    3.30   0.00     8.63    31.56
A    0.02   -1.48    3.30   0.00     8.64    31.58
A    0.02   -1.48    3.30  -0.00     8.64    31.57
A    0.02   -1.48    3.30   0.00     8.64    31.57
A    0.02   -1.48    3.30  -0.00     8.64    31.57
A    0.02   -1.48    3.30   0.00     8.63    31.57
A    0.02   -1.48    3.30  -0.00     8.64    31.57
A    0.02   -1.48    3.30  -0.00     8.64    31.57
g   -6.50    1.37   -8.77  80.25   127.69    -1.39
A    0.02   -1.48    3.30  -0.00     8.64    31.57
A    0.02   -1.48    3.30   0.00     8.64    31.57
A    0.02   -1.48    3.30  -0.00     8.63    31.56
A    0.02   -1.48    3.30   0.00     8.64    31.57
A    0.02   -1.48    3.30  -0.00     8.63    31.58
A    0.02   -1.48    3.30   0.00     8.64    31.56
A    0.02   -1.48    3.30  -0.00     8.64    31.57
A    0.02   -1.48    3.30  -0.00     8.63    31.56
A    0.02   -1.48    3.30   0.00     8.64    31.58
A    0.02   -1.48    3.30  -0.00     8.64    31.57
A    0.02   -1.48    3.30  -0.00     8.63    31.57
```